

This work was written as part of one of the author's official duties as an Employee of the United States Government and is therefore a work of the United States Government. In accordance with 17 U.S.C. 105, no copyright protection is available for such works under U.S. Law.

Public Domain Mark 1.0

<https://creativecommons.org/publicdomain/mark/1.0/>

Access to this work was provided by the University of Maryland, Baltimore County (UMBC) ScholarWorks@UMBC digital repository on the Maryland Shared Open Access (MD-SOAR) platform.

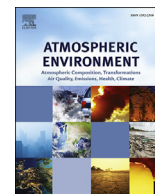
**Please provide feedback**

Please support the ScholarWorks@UMBC repository by emailing [scholarworks-group@umbc.edu](mailto:scholarworks-group@umbc.edu) and telling us what having access to this work means to you and why it's important to you. Thank you.



Contents lists available at ScienceDirect

## Atmospheric Environment

journal homepage: [www.elsevier.com/locate/atmosenv](http://www.elsevier.com/locate/atmosenv)

## Multi year aerosol characterization in the tropical Andes and in adjacent Amazonia using AERONET measurements



Daniel Pérez-Ramírez <sup>a, b, \*</sup>, Marcos Andrade-Flores <sup>c, d</sup>, Thomas F. Eck <sup>e, f</sup>, Ariel F. Stein <sup>g</sup>, Norman T. O'Neill <sup>h</sup>, Hassan Lyamani <sup>a, b</sup>, Santiago Gassó <sup>i, j</sup>, David N. Whiteman <sup>k</sup>, Igor Veselovskii <sup>l, m</sup>, Fernando Velarde <sup>c</sup>, L. Alados-Arboledas <sup>a, b</sup>

<sup>a</sup> Applied Physics Department, University of Granada, 18071, Granada, Spain

<sup>b</sup> Andalusian Institute for Earth System Research (IICTA), Av. Mediterráneo s/n, 18006, Granada, Spain

<sup>c</sup> Laboratory for Atmospheric Physics, Universidad Mayor de San Andrés, La Paz, Bolivia

<sup>d</sup> Department of Atmospheric and Oceanic Sciences, University of Maryland, College Park, MD, United States

<sup>e</sup> Goddard Earth Sciences Technology and Research, University Space Research Association (GESTAR/USRA), 21040, Columbia, MD, United States

<sup>f</sup> Biospheric Sciences Laboratory, NASA Goddard Space Flight Center, 20771, Greenbelt, MD, United States

<sup>g</sup> NOAA Air Resources Laboratory, 5830 University Research Court, 20740, College Park, MD, United States

<sup>h</sup> Centre d'Applications et de Recherches en Télédétection, Université de Sherbrooke, Sherbrooke, Canada

<sup>i</sup> Morgan State University, MD, United States

<sup>j</sup> Climate and Radiation Laboratory, NASA Goddard Space Flight Center, 20771, Greenbelt, MD, United States

<sup>k</sup> Mesoscale Atmospheric Processes Laboratory, NASA Goddard Space Flight Center, 20771, Greenbelt, MD, United States

<sup>l</sup> Joint Center for Earth Systems Technology, University of Maryland Baltimore County, Baltimore, MD, United States

<sup>m</sup> Physics Instrumentation Center of General Physics Institute, Troitsk, Moscow, Russia

## H I G H L I G H T S

- Aerosol in the Bolivian Andes.
- Aerosol transport to high mountains.
- Biomass-burning near the Andes.

## A R T I C L E I N F O

## Article history:

Received 4 March 2017

Received in revised form

17 July 2017

Accepted 19 July 2017

Available online 21 July 2017

## Keywords:

Aerosol in high mountain sites

Aerosol absorption

Aerosol in Amazonia

## A B S T R A C T

This work focuses on the analysis of columnar aerosol properties in the complex geophysical tropical region of South America within 10–20° South and 50–70° West. The region is quite varied and encompasses a significant part of Amazonia (lowlands) as well as high mountains in the Andes (highlands, ~4000 m a.s.l.). Several AERONET stations were included to study the aerosol optical characteristics of the lowlands (Rio Branco, Ji Parana and Cuiaba in Brazil and Santa Cruz in Bolivia) and the highlands (La Paz, Bolivia) during the 2000–2014 period. Biomass-burning is by far the most important source of aerosol in the lowlands, particularly during the dry season (August–October). Multi-annual variability was investigated and showed very strong burning activity in 2005, 2006, 2007 and 2010. This resulted in smoke characterized by correspondingly strong, above-average AODs (aerosol optical depths) and homogeneous single scattering albedo (SSA) across all the stations (~0.93). For other years, however, SSA differences arise between the northern stations (Rio Branco and Ji Parana) with SSAs of ~0.95 and the southern stations (Cuiaba and Santa Cruz) with lower SSAs of ~0.85. Such differences are explained by the different types of vegetation burned in the two different regions. In the highlands, however, the transport of biomass burning smoke is found to be sporadic in nature. This sporadicity results in highly variable indicators of aerosol load and type (Angstrom exponent and fine mode fraction) with moderately significant increases in both. Regional dust and local pollution are the background aerosol in this highland region, whose elevation places it close to the free troposphere. Transported smoke particles were generally found to be more optical absorbing than in the lowlands: the hypothesis to explain this is the significantly higher amount of water vapor in Amazonia relative to the high

\* Corresponding author. Applied Physics Department, University of Granada, 18071, Granada, Spain.

E-mail address: [dperez@ugr.es](mailto:dperez@ugr.es) (D. Pérez-Ramírez).

mountain areas. The air-mass transport to La Paz was investigated using the HYSPLIT air-concentration five-days back trajectories. Two different patterns were clearly differentiated: westerly winds from the Pacific that clean the atmosphere and easterly winds favoring the transport of particles from Amazonia.

© 2017 Elsevier Ltd. All rights reserved.

## 1. Introduction

High mountain areas are very sensitive to climate change as they host many glaciers and are also involved in many cloud formation processes (e.g. Wonsick et al., 2014; Lüthi et al., 2015). Particularly, high mountains in tropical areas are the host of glaciers and snow at such latitudes, irrigating many rivers and thus are essential for the water supply of local population. Changes in glacial and snow covers are indicators of climate change (e.g. Xu et al., 2016). The Andes in South America is the largest mountain chain in the world covering a latitude range from  $-55^{\circ}$  S to  $5^{\circ}$  N and with many peaks above 5000 m a.s.l. The Andes mountain chain is part of many countries and is a natural barrier between the bulk of the South American mainland and the Pacific Ocean. It also represents a fundamental constraint on the eastern meteorology given the predominance of easterly trade winds from the Atlantic Ocean. These trade winds create the conditions for the South American Low Level Jet (SALLJ) that runs parallel to the mountains (Ulke et al., 2011). The SALLJ exhibits an annual cycle that peaks during austral summer and is the major air-mass transport mechanism in South America. Despite its low altitude (around 1500 m a.s.l.), it enhances moisture availability for convection in the Andes Mountains (Nogues-Paegle and Mo, 1997). In other regions containing large mountain chains such as the Himalaya in Asia or the Alps in Europe many studies have been done concerning trace gases (e.g. Schwikowski et al., 1999; Maione et al., 2011), aerosols (e.g. Gautam et al., 2011; Zieger et al., 2012) and cloud formation (e.g. Bonasoni et al., 2010). In the Andes, however, due to the lack of appropriate measurements, these topics have not been studied well.

The Amazon Basin is a major source of anthropogenic-driven biomass-burning emissions (e.g. Mishra et al., 2015), accounting for approximately 15% of total global biomass-burning emissions (van der Werf et al., 2010). Depending on the vegetation burned, fires inject reactive gases, greenhouse gases (e.g. as carbon dioxide ( $\text{CO}_2$ ) and methane ( $\text{CH}_4$ )) and particles into the atmosphere (Andreae and Merlet, 2001; Bowman et al., 2009; Remy and Kaiser, 2014). Biomass-burning emissions are also a major source of organic (14–77 Tg/yr) and black carbon particles (1.8–11 Tg/yr) (e.g. Bond et al., 2013). Aerosol smoke particles that are the result of biomass-burning directly affect the Earth-Atmosphere radiative budget by scattering and absorbing solar radiation (e.g. Jacobson, 2014) and also indirectly by acting as cloud condensation nuclei (CCN) and ice nuclei (IC) and thereby changing the distribution and properties of clouds (e.g. Koren et al., 2008). Biomass-burning can be the cause of serious public health issues such as extreme particulate matter (PM) concentrations caused by fires in the island of Borneo and Sumatra (Eck et al., 2016). Smoke from wildfires has also been associated with both increased mortality (Vedal and Dutton, 2006) and morbidity (Bowman and Johnston, 2005), and may cause ~250,000 (73,000–435,000) premature mortalities/yr, with >90% being associated with PM (Jacobson, 2014).

In Amazonia the smoke emissions caused by agricultural burning of residues (e.g. Uriarte et al., 2009) and by deforestation along the borders of Amazon forests, known as the arc of deforestation (e.g. Morton et al., 2008; Van Marle et al., 2016). The burned areas are commonly found in Brazil, Peru, Colombia, Bolivia,

Paraguay and northern Argentina. Atmospheric transport patterns lead to spatial distributions of smoke that can be very different from the distribution of the actual fire sources (e.g. Freitas et al., 2005). This, in turn, has differing impacts on different environments and populations. As an example, many studies have been carried out over Brazilian areas, including modeling transport efforts (e.g. Matichuk et al., 2008; Longo et al., 2010) and the impact of smoke over both rural areas and highly populated cities (e.g. Reid et al., 1998, 1999; Kotchenruther and Hobbs, 1998). Also, intensive field campaigns such as GOAMAZON (<http://campaign.arm.gov/goamazon2014/>) have been staged to advance the understanding of absorption and aging properties of smoke, of greenhouse gases and of smoke transport patterns. However, due to the enormous areas burned and the population differences as well as different agricultural traditions and agricultural development between Brazil and its neighbors, the study of biomass burning in the rest of South America needs to be the focus of more investigations.

The main objective of this work is to analyze the smoke particle patterns in the Bolivian Andes and surrounding areas. To that end, we focus on the long-term ground-based measurements of the AERONET network acquired at the high mountain site in the city of La Paz (3340 m a.s.l.) and at nearby lowland sites in Brazil and Bolivia. We used the HYSPLIT model (Stein et al., 2015) to interpret the origin of the air masses influencing the study region. Biomass-burning smoke studies using AERONET data have been successfully carried out in Brazil (e.g. Schafer et al., 2008), Africa (e.g. Eck et al., 2003, 2013; Queface et al., 2011) and in Alaska (e.g. Eck et al., 2009) as well as for cases of long-range transport of biomass burning smoke in North America (e.g. Colarco et al., 2003; Veselovskii et al., 2015), Europe (e.g. Alados-Arboledas et al., 2011) and Asia (e.g. Noh et al., 2009). AERONET data on biomass-burning smoke have also been used to improve and validate satellite retrievals (e.g. Sayer et al., 2014).

This work is structured as follows: Section II describes the experimental region and methodology. The results are in Section III and concluding remarks in section IV.

## 2. Experimental region and methodology

The South American study zone of interest is in the tropical region within  $10^{\circ}$ – $20^{\circ}$  South and  $50^{\circ}$ – $70^{\circ}$  West. The area includes three different geophysical regions: The Amazon (lowlands) is characterized by tropical conditions, the high mountain regions by mountains above 6000 m a.s.l. that also include flat areas known as the 'Altiplano' (highlands ~ 4000 m a.s.l.) and by a transition between the two (foothills). Fig. 1 shows a map of the area, including the AERONET stations whose data were used in this study and an example of an elevation profile from the Pacific Ocean to Amazonia crossing the La Paz region. The wet season occurs during the period from December to March, and the dry season is particularly intense in the period from June to September. The most important geo-atmospheric factor is the strong altitude gradient between the lowlands and highlands, with its attendant large differences in water vapor content and relative humidity. The city of La Paz, Bolivia ( $16.36^{\circ}$  South,  $68.06^{\circ}$  West, 3439 m a.s.l.), which is located in a valley surrounded by mountains of up to 5500 m a.s.l. is an

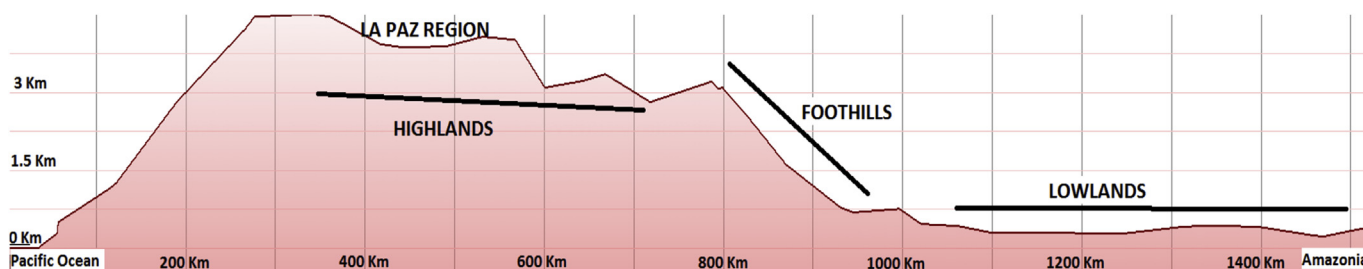


**Fig. 1.** Study region including the AERONET stations used. Horizontal line in the map represents the region of the elevation profile. This figure has been created using Google Earth tools.

important focus of this study. The metropolitan area includes the Andean Altiplano with a total population of around 1.7 million inhabitants. The lowlands to the north and east include the stations of Rio Branco, Brazil ( $9.95^{\circ}$  South,  $67.87^{\circ}$  West, 212 m a.s.l.), Cuiaba, Brazil ( $15.50^{\circ}$  South,  $56.00^{\circ}$  West, 250 m a.s.l.) and Ji-Parana, Brazil ( $10.85^{\circ}$  South,  $61.80^{\circ}$  West, 100 m a.s.l.) These stations are close to small-medium sized cities with populations in the range of 120,000–600,000 inhabitants. The station in the Bolivian city of Santa Cruz de la Sierra ( $17.08^{\circ}$  South,  $63.17^{\circ}$  West, 442 m a.s.l.) with a total population of 2 million was also included in our study. Anthropogenic aerosol emissions from these cities, particularly

road traffic emissions, are the main sources of local anthropogenic aerosol over the study region.

Column-integrated characterization of atmospheric aerosol was examined using AERONET sun-photometry measurements. The standard AERONET instrument is the well-known CIMEL CE-318-4 sun photometer. This device measures direct sun signals at 340, 380, 440, 500, 675, 870, and 1020 nm which are transformed into aerosol optical depths (AODs). Details of AERONET sun photometers including calibration, error analysis and aerosol optical properties retrievals are in Holben et al. (1998), Eck et al., (1999) and in Smirnov et al. (2000). All the data used in this study are cloud-



screened and quality assured (Level 2.0).

Within the solar spectrum, the Angström exponent is a good indicator of the predominant size of atmospheric particles (i.e. Dubovik et al., 2002):  $\alpha > 1.5$  implies the predominance of fine mode (submicron) aerosols while  $\alpha < 0.5$  implies the predominance of coarse mode (supermicron) aerosols. However, for a more accurate characterization of the relative influence of fine and coarse mode particles an interpretation based solely on very high or very low values of  $\alpha$  is not straightforward. We accordingly used the Spectral Deconvolution Algorithm (SDA) product incorporated into AERONET standardized processing (O'Neill et al., 2001a,b; 2003), to study fine mode AOD ( $AOD_{\text{fine}}$ ), coarse mode AOD ( $AOD_{\text{coarse}}$ ), and fine mode fraction ( $\eta = AOD_{\text{fine}}/AOD$ ) at a reference wavelength of 500 nm.

In terms of aerosol microphysical properties, the operational AERONET algorithm (Dubovik and King, 2000; Dubovik et al., 2002) uses sky radiances and direct sun measurements as inputs and provides retrieved aerosol size distribution as well as intensive properties such as aerosol refractive index, single scattering albedo (SSA) and asymmetry factor ( $g$ ) (across four spectral bands at 440, 675, 870, 1020 nm). However, the AERONET algorithm has specific and often difficult to satisfy sky condition requirements (Holben et al., 2006) in that skies must be completely clear and large scattering angles (typically larger than  $50^\circ$ ). These limitations imply that refractive index retrievals are only reliable for  $AOD > 0.4$ , although not for the retrieval of size distribution (Holben et al., 2006). It accordingly provides low temporal resolution results (generally a maximum of approximately 8 inversions per day are possible). Nevertheless, retrievals that uses sky radiance measurements are the only that are able to provide retrieved values of aerosol refractive index, single scattering albedo and phase function with appropriate accuracy (Dubovik et al., 2006).

To complement AERONET retrieved aerosol microphysical properties, we compute additional retrievals using the Linear Estimation (LE) technique (Veselovskii et al., 2012, 2013), that uses AERONET spectral AODs measurements as input to yield high frequency estimates of aerosol microphysical parameters during the whole day. The parameters retrieved using the LE technique are the effective radius ( $r_{\text{eff}}$ ) and the volume concentration ( $V$ ). The other retrievals we ran were based on the method proposed by O'Neill et al. (2005, 2008a), which, itself, is based on the spectral curvature of the fine mode Angstrom slope and its spectral derivative, derived from the SDA. This algorithm is used to estimate the fine mode effective radius ( $r_{\text{fine}}$ ).

The inversions by LE are constrained in the maximum radius allowed in the inversion due to the range of AODs used (380–1020 nm), being improved the retrieval accuracy. Measurements of  $\alpha(440\text{--}870)$  are used for the selection of the maximum radius in the inversion, being of  $2\text{ }\mu\text{m}$  for fine mode predominance and of  $10\text{ }\mu\text{m}$  for the rest of cases. Also, simulations revealed that LE retrievals have an accuracy below 20% for  $r_{\text{fine}} > 0.12\text{ }\mu\text{m}$ , while the accuracy degrades for lower  $r_{\text{fine}}$  due to the lack of sensitivity of the inversion range to these tiny particles. Posterior comparisons versus AERONET retrievals showed differences of up to 10% for fine mode predominance and 20% for coarse mode predominance. The largest uncertainties were found for mixtures of both modes with differences up to 30%. Because the use of LE retrievals is for supporting AERONET inversions, corrections functions are applied which reduced the differences between the two retrieval schemes to generally less than 10%. We remark here that AERONET uncertainties are similar to these ranges (Dubovik et al., 2002). More details about the use of Linear Estimation retrievals are in Pérez-Ramírez et al. (2015). On the other hand, for the retrievals of  $r_{\text{fine}}$  using O'Neill et al. (2005, 2008a) methodology, comparisons versus AERONET retrievals for the limited data set of O'Neill et al. (2005)

and confirmed by more recently unpublished AERONET-wide comparisons show average differences  $\sim 10\%$  for  $\eta$  values  $> \sim 0.5$ .

The HYSPLIT model (Stein et al., 2015), developed by the NOAA Air Resources Laboratory and accessible on-line at <http://www.ready.noaa.gov/HYSPLIT.php>, is used to compute air parcel backward-trajectories and from them assess dispersion of aerosols. The meteorological data used to run the model were from 6-hourly GDAS (Global Data Assimilation <http://www.emc.ncep.noaa.gov/gmb/gdas/>) output at  $1^\circ$  degree horizontal resolution. The total trajectory time was set to 120 h.

### 3. Results

#### 3.1. Aerosol optical properties

Fig. 2 shows the temporal evolution of daily means of AOD,  $AOD_{\text{fine}}$  and  $AOD_{\text{coarse}}$  for the AERONET stations, whose data were employed in our study (with a zoomed insert of the temporal plot of the highlands station of La Paz). The reference wavelength is 500 nm. Table 1 presents a statistical summary of the parameters in Fig. 2, particularly mean values, standard deviations (STD), medians, maxima and minima.

Maxima of AOD,  $AOD_{\text{fine}}$  and  $AOD_{\text{coarse}}$  occur during the biomass-burning season from August to October. The intensity of the biomass-burning season varies from year to year as evidenced, for example, by the different maximum values of Fig. 2. These intense biomass-burning seasons have also been reported in the literature based on satellite observations (e.g. Torres et al., 2010). During the biomass-burning season, increases in  $AOD_{\text{fine}}$  and  $AOD_{\text{coarse}}$  are observed when compared with other seasons. But the increase of  $AOD_{\text{fine}}$  is very large compared to that of  $AOD_{\text{coarse}}$ , indicating a large predominance of fine particles (by about an order of magnitude).

The differences in the maximum values of AODs among the different biomass-burning seasons imply a multi-year variability in fire emissions, which is consistent with the large standard deviation of AODs reported in Table 1. Emissions of smoke particles from biomass burning are mostly associated with human activities. Examples of this are fires that are used for forest clearing by small farmers and plantation owners who clear understory shrubbery and cut forest trees. The area is burned a few months after the clearing, and, although the fires are intended to only burn in limited areas, they sometimes spread beyond the targeted agricultural zone and consume pristine rainforest (e.g. Torres et al., 2010). The extent and intensity of the burned areas can vary from year to year.

To show that the data used are predominately cloud-free, Fig. 3 shows  $\alpha(440\text{--}870)$  versus  $AOD(500)$  for lowland stations. Cloud-affected data typically present  $\alpha(440\text{--}870) < 0.5$  (O'Neill et al., 2003). In particular, AODs  $> 2$  are associated with  $\alpha(440\text{--}870)$  values that are generally  $> 1.2$ , a value which suggests minimal cloud contamination in the measurements. Moreover, the number of photocounts is large enough to guarantee the quality of the measurements: for very high AODs the number of photocounts registered by the AERONET instruments ranged from about 50 to 20 counts for 500 nm AODs of 4 and 6 respectively at the Cuiaba site, while the minimum count required for good AOD measurement is 10 (Sinyuk et al., 2012).

The analyses of  $\eta$  is also useful for detecting when AOD measurements are affected by thin and stable cirrus clouds (O'Neill et al., 2003). Measurements affected by cirrus clouds present low  $\eta$  because these clouds are formed by big ice crystals. Indeed, for aerosol with fine mode predominance and not affected by cirrus  $\eta$  present high values. This approach can be applied for smoke particles. The analyses performed of  $\eta$  values for Fig. 3 data reveal that measurements with  $AOD > 2.0$  (71 days totally) present  $\eta > 0.85$ ,

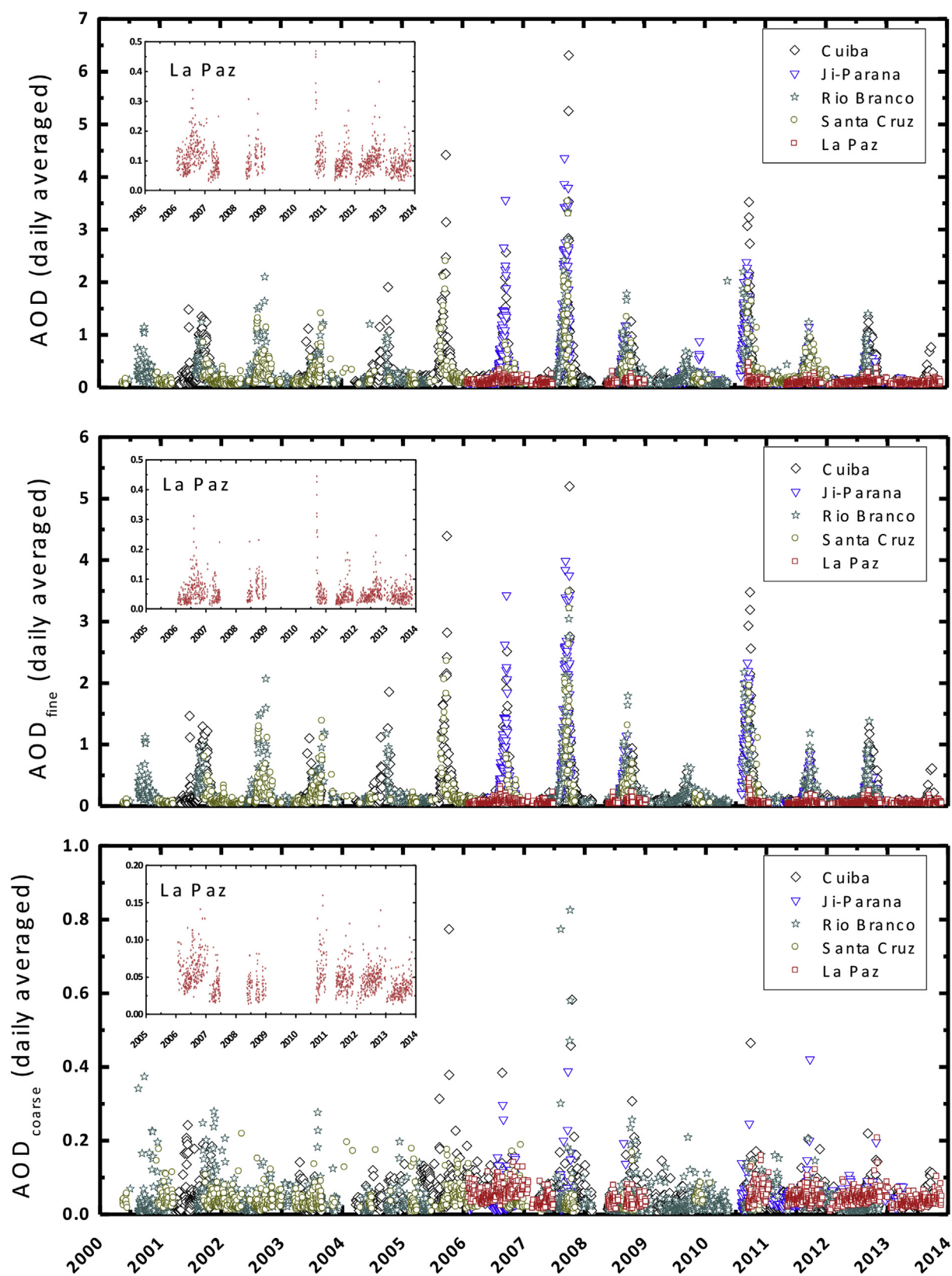


Fig. 2. Temporal evolution of daily averaged AOD, including these of the fine and coarse mode. Reference wavelength is 500 nm.

**Table 1**

Mean, standard deviation (STD), median and maximum (Max.) and minimum (Min.) values of aerosol optical depth (AOD), Angstrom parameter ( $\alpha$ ) between 440 and 870 nm, fine (AOD<sub>fine</sub>) and coarse (AOD<sub>coarse</sub>) mode aerosol optical depths and relative contribution of fine mode to total optical depth ( $\eta$ ). Data are presented for biomass and non biomass-burning seasons for the stations in the lowlands (Cuiaba, Ji Parana, Rio Branco and Santa Cruz) and in the highlands (La Paz). Reference wavelength for AOD, AOD<sub>fine</sub>, AOD<sub>coarse</sub> and  $\eta$  is 500 nm.

		AOD	Alpha	AOD <sub>fine</sub>	AOD <sub>coarse</sub>	Eta	AOD	Alpha	AOD <sub>fine</sub>	AOD <sub>coarse</sub>	Eta
		Biomass-Burning Season					No Biomass-Burning Season				
Cuiaba	Mean	0.55	1.56	0.48	0.06	0.82	0.13	1.15	0.08	0.04	0.64
	STD	0.61	0.30	0.55	0.06	0.14	0.09	0.32	0.08	0.03	0.14
	Median	0.35	1.63	0.29	0.05	0.85	0.11	1.15	0.07	0.04	0.64
	Max.	6.31	2.12	5.20	0.77	0.99	0.21	2.15	0.19	0.24	0.99
	Min.	0.07	1.41	0.03	0.00	0.24	0.03	0.95	0.01	0.00	0.54
Ji Parana	Mean	0.89	1.71	0.80	0.05	0.89	0.13	1.15	0.06	0.04	0.58
	STD	0.79	0.25	0.79	0.05	0.12	0.09	0.29	0.04	0.02	0.11
	Median	0.50	1.75	0.50	0.04	0.93	0.11	1.14	0.05	0.04	0.57
	Max.	4.36	2.15	3.99	0.42	0.99	0.24	1.97	0.20	0.16	0.89
	Min.	0.07	1.55	0.04	0.01	0.54	0.03	0.95	0.01	0.01	0.20
Rio Branco	Mean	0.52	1.67	0.47	0.04	0.89	0.11	0.84	0.09	0.04	0.72
	STD	0.46	0.29	0.45	0.07	0.12	0.08	0.31	0.06	0.03	0.15
	Median	0.36	1.74	0.31	0.02	0.93	0.09	0.82	0.08	0.02	0.75
	Max.	3.53	2.40	3.22	0.92	0.99	0.19	1.92	0.15	0.18	0.98
	Min.	0.06	1.54	0.04	0.01	0.22	0.02	0.62	0.02	0.00	0.20
Santa Cruz	Mean	0.52	1.64	0.53	0.04	0.87	0.13	1.31	0.09	0.05	0.64
	STD	0.53	0.25	0.57	0.03	0.12	0.09	0.37	0.09	0.02	0.16
	Median	0.33	1.69	0.29	0.03	0.92	0.11	1.36	0.06	0.03	0.64
	Max.	3.53	2.15	3.48	0.17	0.99	0.24	2.4	0.20	0.21	0.98
	Min.	0.06	1.49	0.05	0.00	0.18	0.03	1.05	0.01	0.01	0.17
La Paz	Mean	0.12	0.95	0.07	0.05	0.55	0.09	0.84	0.04	0.04	0.48
	STD	0.06	0.30	0.06	0.02	0.15	0.04	0.31	0.03	0.02	0.13
	Median	0.11	0.95	0.05	0.05	0.53	0.08	0.82	0.04	0.04	0.48
	Max.	0.46	1.69	0.44	0.13	0.95	0.16	1.92	0.14	0.08	0.89
	Min.	0.03	0.74	0.01	0.01	0.17	0.02	0.62	0.01	0.01	0.17

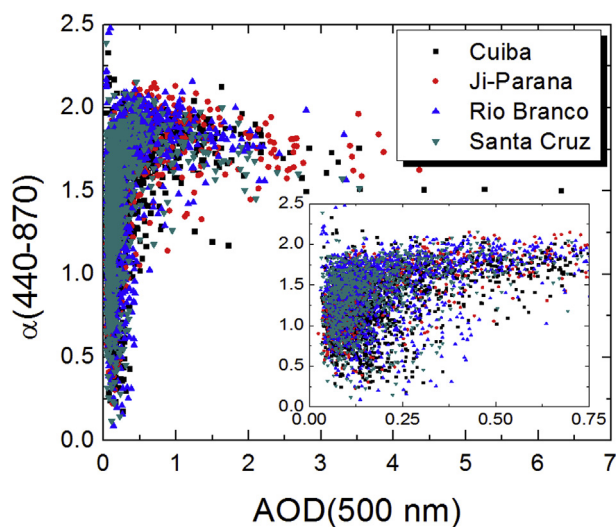


Fig. 3. Angstrom exponent versus AOD for the measured points of Fig. 2.

suggesting no presence of clouds. For  $1 < \text{AOD} < 2$  were registered 220 days of measurements, and it is found that 94% with  $\eta > 0.9$ , and only 4 days of measurements with  $\eta < 0.75$  that could be associated with influence of thin cirrus clouds. Finally, for 394 days of measurements that presented  $0.5 < \text{AOD} < 1$ , were registered 82% of cases with  $\eta > 0.9$  and 94% with  $\eta > 0.8$ . The rest of the cases with lower  $\eta$  can be associated with aerosol influenced by coarse particles, although the presence of thin cirrus clouds cannot be discarded.

The maximum values reported in Fig. 2 represent some of the largest values ever registered in the AEROENT Version 2 database ([http://aeronet.gsfc.nasa.gov/cgi-bin/climo\\_menu\\_v2\\_new](http://aeronet.gsfc.nasa.gov/cgi-bin/climo_menu_v2_new)). The

mean values during the biomass-burning season are also among the largest monthly mean climatological values. Schafer et al. (2008) registered similar values using stations located in the Amazon basin. Comparably high AOD values were also reported for African biomass-burning by Eck et al. (2003, 2013). Moreover, the occurrence of very high AOD values over the extended periods of time that we have reported here are only obtained in very polluted parts of Asia (e.g. Eck et al., 2010), very dusty areas in the Sahara (e.g. Guirado et al., 2014) and the Arabian Peninsula (e.g. Kim et al., 2011).

For the highland La Paz station the AOD increased during the August–October period from mean values around 0.09 to 0.12 (Table 1), but the AOD values are much lower than those in the lowlands. Although the fine mode is still predominant, the contribution of coarse mode to the total AOD cannot be ignored. The frequency histograms of AOD(500) for each station are given in Fig. 4, and they show that only 7% of data at La Paz present  $\text{AOD} > 0.4$  while for the stations of Cuiaba, Ji Parana, Rio Branco and Santa Cruz these percentages are of 45%, 59%, 44% and 41% respectively. That indicates the greater contribution of biomass-burning particles in the lowlands to the total aerosol load and to the aerosol seasonal changes.

Multi-wavelength lidar measurements in the central Amazon made by Baars et al. (2012) showed that smoke plumes can reach altitudes up to 5 km. During the burning season, the reduced vegetation in the highlands implies few fires, while the large AODs in the lowlands suggests that transport of smoke particles from nearby Amazonia is a important source of particles in the highlands. The Andes chain in the tropics is therefore a barrier for the transport of smoke to the Pacific Ocean, in agreement with the results of Bourgeois et al. (2015) using CALIPSO data.

Indicators of particle type predominance between biomass and non-biomass burning seasons is illustrated in Fig. 5, where Box-Whisker plots of  $\alpha(440-870)$  and fine mode fraction are represented. In the Box-Whisker plots, the mean is represented by a very

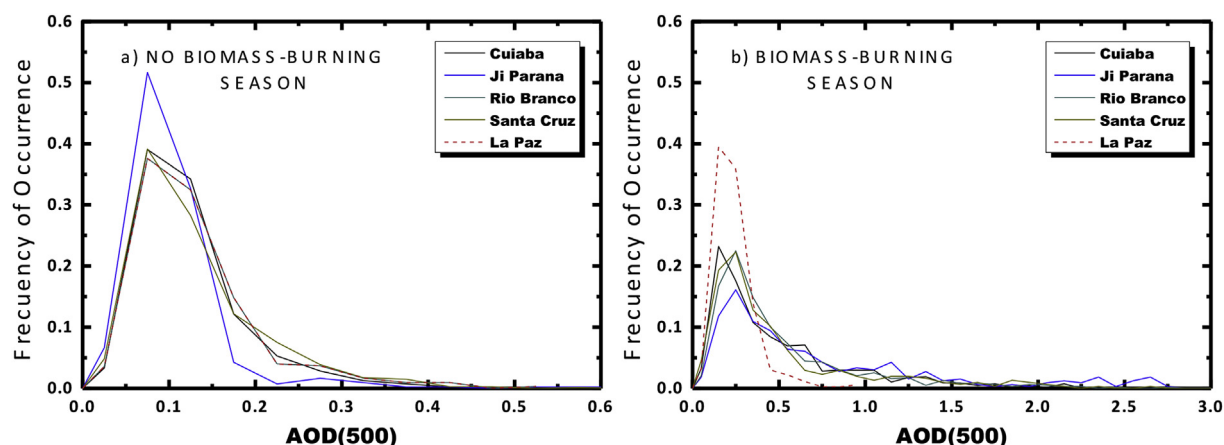


Fig. 4. Frequency histograms of aerosol optical depth at 500 nm (AOD(500)) for (a) no biomass-burning and (b) biomass-burning seasons.

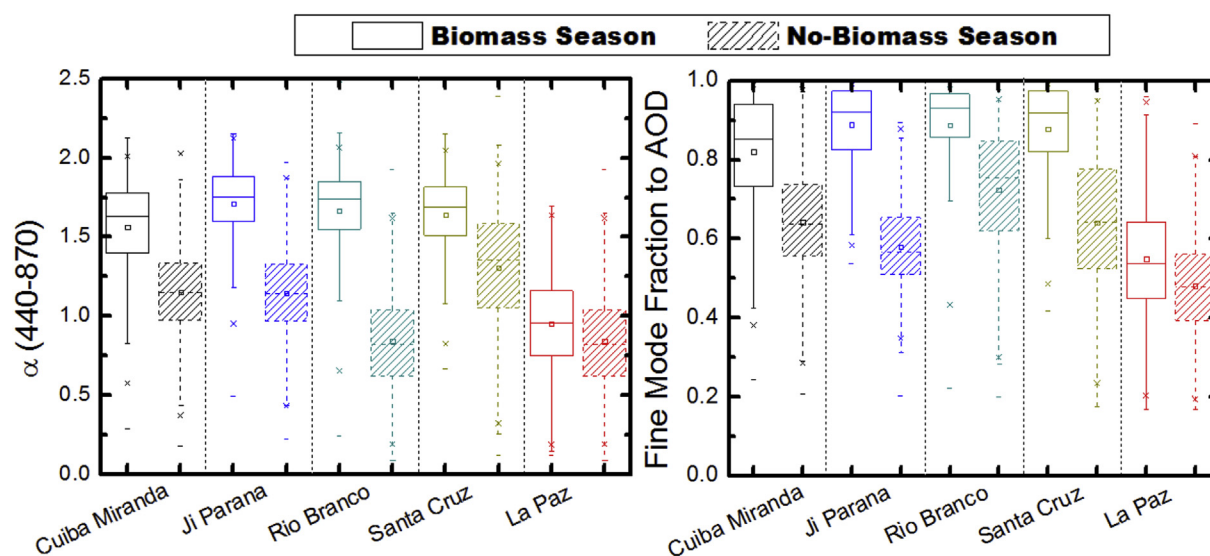


Fig. 5. Box-Whisker plots during the biomass and no biomass-burning seasons of the Angstrom parameter  $\alpha(440-870)$  and fine mode fraction to AOD for the lowlands stations (Cuiaba Miranda, Ji Parana, Rio Branco and Santa Cruz) and the highlands station (La Paz). In the Box-Whisker plots, the mean is represented by a very small open square within a given rectangle. The horizontal line segment in the rectangle is the median. The top limit (top of the rectangle) represents the 75th percentile (P75) and the bottom limit the 25th percentile (P25). The lines perpendicular to the boxes are the 1st (P1) and 99th (P99) percentiles, and the crosses represent the maximum and minimum values respectively.

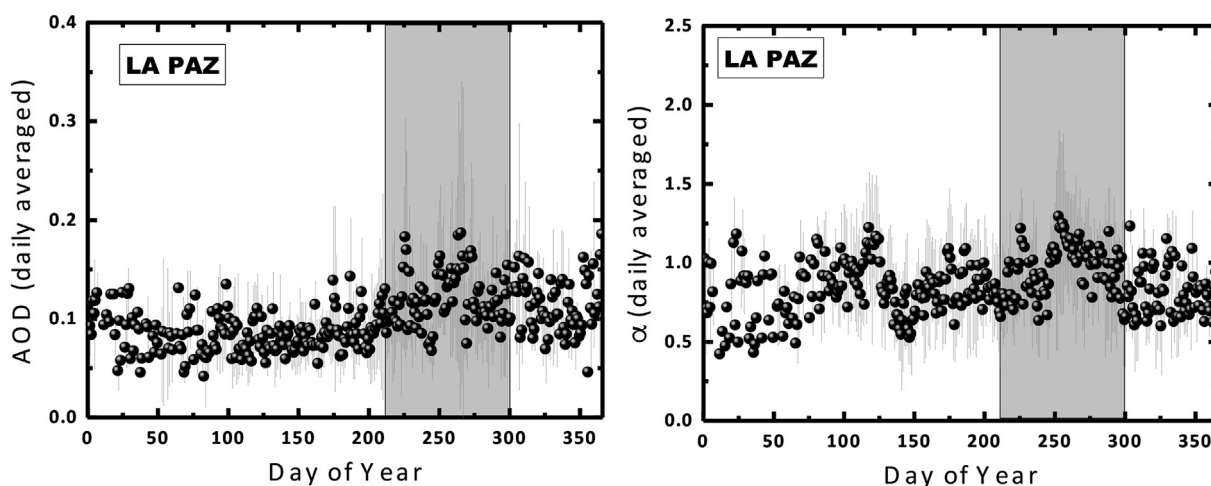
small open square within a given rectangle. The horizontal line segment in the rectangle is the median. The top limit (top of the rectangle) represents the 75th percentile (P75) and the bottom limit the 25th percentile (P25). The lines perpendicular to the boxes are the 1st (P1) and 99th (P99) percentiles, and the crosses represent the maximum and minimum values respectively.

Fig. 5 shows very high values of  $\alpha(440-870)$  in the lowlands during the biomass-burning seasons, with mean values of 1.5–1.7 which are similar to biomass-burning values reported in the literature (e.g. Dubovik et al., 2002; Schafer et al., 2008) and, along with the values of  $\eta$  above 0.80, indicate a predominance of fine particles. Lower values of  $\alpha(440-870)$ , characterized by large standard deviations, are observed for the non-biomass burning seasons. The mean values also vary significantly among stations (from 0.86 at Rio Branco to 1.36 at Santa Cruz). These results, plus the fact that the values of  $\eta$  vary between 0.7 and 0.5, indicate a lack of predominance of fine or coarse mode in the wet season. Indeed, a mixture of different particles predominates. On the other hand, the mean Angstrom Exponent values of 0.94 and 0.85 for the biomass and non-biomass burning seasons, respectively at the highland station

of La Paz, are not significantly different after considering the standard deviation. The same is true for  $\eta$ , with mean values of 0.55 and 0.48 respectively. These La Paz values of  $\alpha(440-870)$  and  $\eta$  cannot, accordingly, be associated with large predominance of either fine or coarse mode.

The multi-year and seasonal variability of AOD and  $\alpha(440-870)$  in the highland station is illustrated in Fig. 6 as a function of the day of the year. Mean values are represented by dots and standard deviations by vertical lines. These values are the result of averaging AOD for each day of the year in different years. During the biomass-burning season mean AOD at 500 nm is of  $0.12 \pm 0.06$ , but the standard deviations indicate AOD peaks of up to 0.35, and are typical values associated with the transport of biomass-burning particles to high mountain places (e.g. Pérez-Ramírez et al., 2008). For other high mountain sites in the Himalayas during the pre-monsoon season, values of up to 0.1 are reported at elevations of ~5000 m a.s.l. (Marcq et al., 2010) and up to 0.5 at elevations of ~2000 m a.s.l. (Dumka et al., 2008). Therefore, the values obtained in La Paz station are similar to high-mountain Himalayan sites affected by the transport of pollutants. The large standard





**Fig. 6.** Mean AOD and Angstrom parameter ( $\alpha(440-870)$ ), including standard deviations, for every day of the year for the highland station of La Paz. The areas shadowed in light grey represent the biomass-burning seasons.

deviations of AODs in the biomass-burning season also indicate large variability, which suggests that the arrival of smoke particles occurs during sporadic events rather than as part of a continuous. AODs values during the other seasons (especially in the April–July period), are  $\sim 0.1$  and are considered as background conditions (local origins). Therefore, biomass-burning transport to high mountains can induce AOD values of up to five times the average background conditions. In section 3.4, we study examples of such events in detail. The period November–March (wet season) exhibits large variability, which might be explained by meteorological factors such as wet deposition and by the less robust statistics of the smaller database associated with that period.

The parameter  $\alpha(440-870)$  shows mean values that are not significantly different during the biomass burning season as compared with the other seasons (Fig. 6b). This suggests that the particle type predominance during the biomass-burning season is similar to that in other seasons (which are probably dominated by aerosols of local origin). Actually, during the biomass-burning season, mean  $\alpha(440-870)$  values are around 1.0 while values for background conditions (focussing on the April–July period with mean AODs of  $\sim 0.09$ )  $\alpha(440-870)$  are around 0.85. In the wet season (November–March), the larger variability observed in Fig. 6 can be explained by the low AODs ( $<0.05$ ) which implies larger uncertainties in  $\alpha(440-870)$ .

The frequency of sporadic smoke events transported to La Paz can be observed in the  $\alpha(440-870)$  versus AOD graph of Fig. 7 (whose dataset is limited to the biomass-burning season). In order to discriminate AOD contributions associated with the transport of smoke from background AODs, we established  $\text{AOD} > 0.14$ , which is the mean plus standard deviation value during the non biomass-burning season (Table 1), as a criterion for classifying intense smoke events. Analyses of Fig. 7 data indicate that only 10% of the measurements acquired during the biomass-burning season exceed this threshold. The cases of smoke transport are characterized by a considerably higher  $\alpha(440-870)$  ( $1.4 \pm 0.2$ ) versus the background. Since there is no other extra source than episodic biomass-burning aerosols (emissions by local sources are almost constant throughout the year), the large differences in the Angstrom exponent associated with smoke between lowlands ( $\sim 1.8$ ) and highlands ( $\sim 1.4$ ) suggest changes in smoke particles during their transport to the highlands. This could also suggest a larger influence of local coarse mode particles at La Paz since the

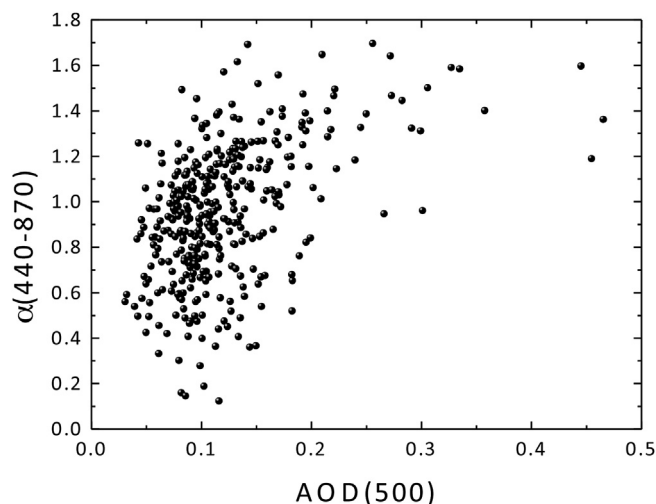


**Fig. 7.** Angstrom exponent versus AOD in the highlands station of La Paz.

maximum AOD values are much lower there than in the Amazonian Basin.

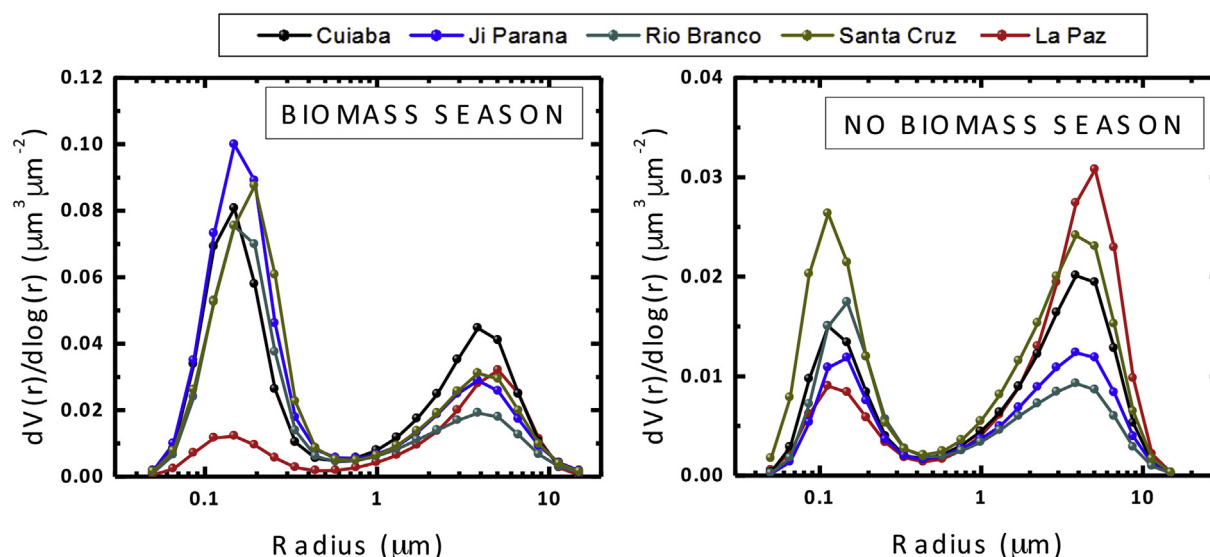
### 3.2. Biomass-burning and precipitation rates

Table 2 reports the rainfall difference between registered and climatological values for each season. Such difference is defined here as rainfall anomaly. Data used are from TRMM satellite (<http://trmm.gsfc.nasa.gov>) for the period 2002–2014 in the study area ( $10-20^\circ$  South,  $50-70^\circ$  West.). The mean of the TRMM data are taken as the climatological values and are shown in parentheses. The ‘wet’ period was taken to be November–March, the ‘dry’ period to be April–July while the biomass burning period was taken as August–October.

An anomalous precipitation increase during the wet period can increase the amount of vegetation to be burned during the biomass-burning season (Uhl et al., 1998). Increases in precipitation during the biomass-burning period favors particle wet deposition and the shortening of aerosol lifetimes (Freitas et al., 2005). An increase in aerosol loads can be expected for the dry and biomass

**Table 2**  
Precipitation anomaly for 'wet' (November–March), 'dry' (April–July) and biomass-burning seasons (August–October). The mean climatological values are in parentheses. The anomaly is defined as the difference between registered and climatological values for each season. All precipitation data were acquired by the TRMM satellite and are the average over the area 10–20° South and 50–70° West. The AOD column is the average, at 500 nm, across the biomass burning season for the lowland stations at Cuiaba, Ji Parana, Rio Branco and Santa Cruz. The "Wet" column represents data whose November to March period started in the previous year.

	Rainfall Anomaly (mm) for different seasons			Mean AERONET AOD during Biomass-Burning Season
	Wet (199.70 mm)	Dry (42.97 mm)	Biomass-Burning (67.16 mm)	
2000	2.74	−3.64	−2.06	0.39 ± 0.29
2001	−9.46	3.56	4.74	0.47 ± 0.30
2002	−16.16	1.91	−5.02	0.49 ± 0.37
2003	−20.75	2.81	12.32	0.42 ± 0.27
2004	−2.97	−4.99	−4.35	0.44 ± 0.38
2005	12.08	−4.05	5.28	0.80 ± 0.70
2006	1.69	−9.01	0.72	0.62 ± 0.59
2007	35.70	−12.51	−6.5	1.18 ± 1.00
2008	9.20	−12.07	−1.30	0.43 ± 0.29
2009	10.02	7.27	0.17	0.20 ± 0.11
2010	3.41	−11.91	−5.91	0.95 ± 0.67
2011	5.77	−11.57	−6.70	0.32 ± 0.21
2012	−13.08	7.28	−12.94	0.40 ± 0.27
2013	41.18	9.13	15.94	0.29 ± 0.19



**Fig. 8.** Mean columnar volume size distributions for the lowland stations and highland (La Paz), both for biomass and no biomass-burning seasons.

burning periods due to unusually dry conditions that intensify fire activity. Such links with precipitation seem to be clear for the intense biomass-burning activity (as represented by AOD amplitude in Fig. 2) registered in 2005–2010: positive rainfall anomalies in the wet season could have increased the amount of biomass that could be burned in the following burning season, while negative rainfall anomalies in the dry and/or burning seasons could have favored fire activity. An exception to this pattern is 2009, which exhibits positive rainfall anomalies during the dry and biomass-burning seasons and therefore lowers AODs. However, in 2008 a strange behavior was observed in that dry conditions were present but lower AOD values were recorded compared with 2005, 2006, 2007 and 2010. The strange behavior in 2008 was also reported by Torres et al. (2010) using OMI space-borne sensor data.

The 2002–2004 period (except for the dry period of 2004) exhibits an opposite pattern, with a precipitation deficit in the wet season and positive rainfall anomalies in the dry and burning seasons. The lower AODs for these years are broadly coherent with the concepts presented above on the relationship between rainfall anomaly and fire activity. However, after 2011 the type of reasoning

that we have employed above to make the link between rainfall anomaly and fire activity is not followed, as a continuous reduction of AODs and fire activity has been observed independently of precipitation. Specific regulations and/or economic forces as suggested by Koren et al. (2007, 2009) could have helped to reduce fire activity. More years of data and perhaps different level of correlation analyses have to be investigated.

### 3.3. Aerosol particle sizes

Fig. 8 shows the mean particle volume size distributions from AERONET almucantar retrievals for the study stations, separated into biomass and non-biomass burning seasons. Different scales are used in the Y-axes between both seasons to better visualize size distribution shapes. This figure indicates that during the biomass-burning season the fine mode largely predominates for the lowland stations. Very similar size distributions for biomass-burning have been reported in the literature (e.g. Eck et al., 2003; Schafer et al., 2008). However, in the highlands the size distribution exhibits two modes with approximately the same volumetric

relevance, although that does not imply that both modes have the same optical effect (in the visible spectral range, for the same volume,  $AOD_{fine}$  is larger than  $AOD_{coarse}$ ). This is broadly consistent with the previous results of the  $\alpha(440-870)$  and  $\eta$  analysis: the coarse mode could be associated with the injection of dust particles from the Andean Altiplano, either by traffic re-suspension or regional winds: On-going studies with in-situ instrumentation are revealing that 50% of PM10 particles are associated with mineral dust (Alastuey, 2017). Fine mode particles are likely associated with anthropogenic activity (e.g. vehicle emissions) and with the transport of smoke particles. On the other hand, during the non-biomass burning season, the maxima of volume size distributions are lower in accordance with the lower AODs. It is also observed for all the stations that no mode predominates, but rather, there is an apparent mixture of different types of particles. This result is also consistent with the intermediate values of  $\alpha(440-870)$  and  $\eta$  noted above. For La Paz, the two modes are explained by the same mechanism noted for the biomass-burning case, although the fine mode volume is smaller due to the absence of transported smoke particles.

The stations in the lowlands, Santa Cruz and Cuiaba show a relevant coarse mode, which is present in both seasons. This coarse mode can be associated with different local sources of dust. Transport of dust from river beds is a possible explanation, as is illustrated in Fig. 9 which shows a true color image for the lowland area on 12th September 2016. The image is composed by the different images acquired by MODIS (Aqua and Terra) and VIIRS space systems (images available at <http://go.nasa.gov/2eULwP1>). The low level jet which runs parallel to the mountain with southerly direction is observed from the clouds and smoke transport patterns. Making a zoom on the river areas, transported dust

plumes are observed. Injections of dust from riverbeds have been also observed in Alaska (Crusius et al., 2011). In South America, other regions that could be responsible for transport of dust to the lowlands is the Chaco plain that spreads to the Andes foothills through Bolivia, Argentina and Paraguay, and include some of the largest tributary rivers and delta rivers in the world (Latrubesse et al., 2012). From more southern locations, injections of salt particles in the atmosphere have been observed from the Mar Chiquita Lake (Boucher and Stein, 2016). The Andean region has other possible sources of dust particles such as the Salar de Uyuni or the Atacama Desert (Gaiero et al., 2013). The high latitudes of these two places could have more influence on the injection of particles in the lowlands. Nevertheless, more analysis is needed to study the impact and properties of dust particles in the tropical region of South America.

Measurements of water vapor mixing ratio,  $w$ , derived from different meteorological stations in Bolivia are available for more than 10 years, both for the lowlands and the highlands. For the wet period (November–March) when most precipitation occurs, the highest values of  $w$  are found (around 19 g/Kg and 8 g/Kg for the lowlands and highlands, respectively). For the dry period (April–July) with very little precipitation the lowest values are found (around 14 g/Kg and 4 g/Kg for the lowlands and highlands, respectively). However, for the biomass-burning season values are in the middle (around 16.5 g/Kg and 5.5 g/Kg for the lowlands and highlands, respectively) indicating the presence of enough water vapor in the atmosphere to favor cloud development which therefore, reduces the number of measurements that fulfil the completely cloud-free sky AERONET criteria for retrieving aerosol microphysical properties. Therefore, due to AODs measurements only require direct sun measurements, LE retrievals and O'Neill

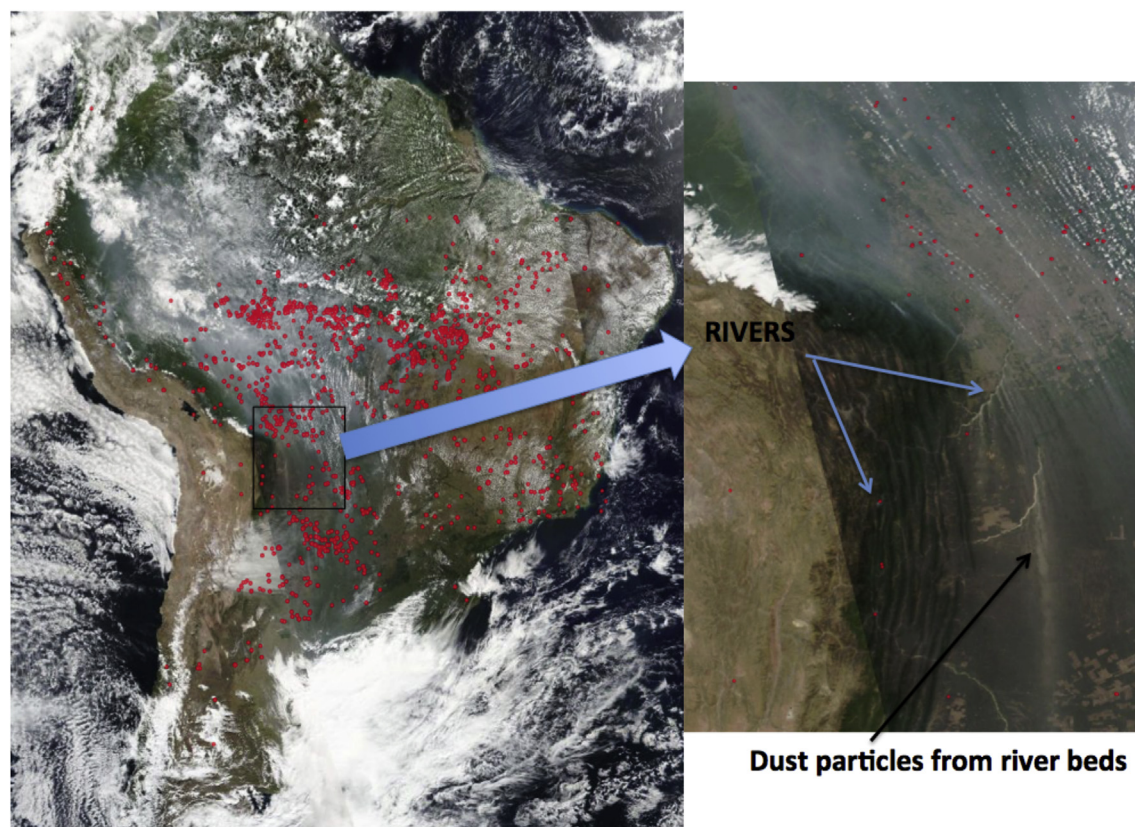


**Fig. 9.** True color image of South America from the composition of images from MODIS (Aqua and Terra) and VIIRS space-systems for 12th September 2016. A zoom is made on the lowlands in Bolivia.



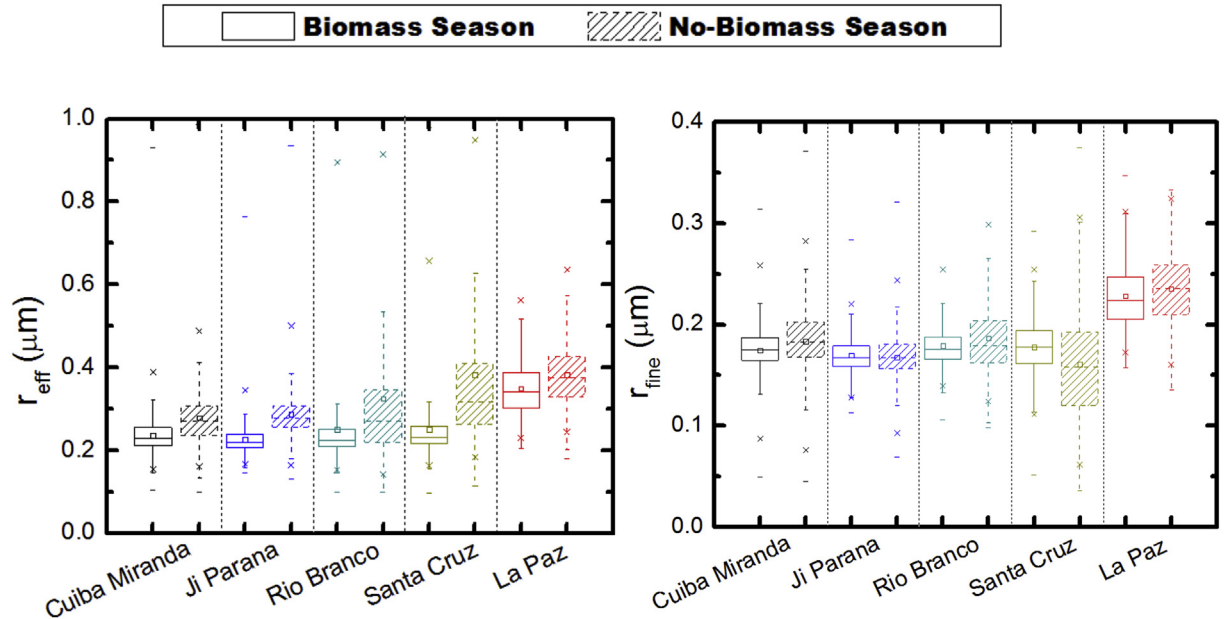


**Fig. 10.** Box-Whisker plots during the biomass and no biomass-burning seasons of the effective radius ( $r_{eff}$ ) and fine mode effective radius ( $r_{fine}$ ) for the lowland stations (Cuiaba Miranda, Ji Parana, Rio Branco and Santa Cruz) and the highland station (La Paz). In the Box-Whisker plots, the mean is represented by a very small open square within a given rectangle. The horizontal line segment in the rectangle is the median. The top limit (top of the rectangle) represents the 75th percentile (P75) and the bottom limit the 25th percentile (P25). The lines perpendicular to the boxes are the 1st (P1) and 99th (P99) percentiles, and the crosses represent the maximum and minimum values respectively.

et al. (2005) methodology are used to obtain  $r_{eff}$  and  $r_{fine}$ , respectively, and complement AERONET retrievals. Actually, during all of the biomass-burning seasons, the number of Level 2.0 retrievals obtained using the almucantar retrieval was 738, 750, 1017, 262 and 206 for the Rio Branco, Ji Parana, Cuiaba, Santa Cruz and La Paz stations, respectively. The number of higher temporal resolution (spectral) retrievals using the LE technique were respectively 16189, 6343, 25017, 6719 and 18220 – this is a significant increase in the number of retrievals for the La Paz station compared with the AERONET almucantar retrievals.

To understand the spatial differences in retrieved particle radii, station by station, Box-Whisker plots of  $r_{eff}$  and  $r_{fine}$ , separated into biomass-burning and non biomass-burning seasons, are shown in Fig. 10. Table 3 summarizes the main statistical parameters of these plots. Linear Estimation and O'Neill et al. (2005) retrievals are used. Similar patterns and statistics were obtained using only AERONET retrieval data, although less robust statistically. During the biomass-burning season the similarity of the mean values and the low standard deviations of both parameters in the lowlands is remarkable: both of these comparisons indicate an approximate

**Table 3**  
Mean, standard deviation (STD), median and maximum (Max.) values of effective radius ( $r_{eff}$ ) and effective radius of the fine mode ( $r_{fine}$ ). Data are presented for biomass and no biomass-burning seasons for the lowland stations (Cuiaba, Ji Parana, Rio Branco and Santa Cruz) and the highlands (La Paz).

		$r_{eff}$		$r_{fine}$	
		Biomass-Burning		No Biomass	
Cuiaba	Mean	0.24	0.18	0.27	0.20
	STD	0.05	0.03	0.07	0.04
	Median	0.23	0.18	0.27	0.20
	Max.	0.93	0.31	0.99	0.38
Ji Parana	Mean	0.22	0.17	0.29	0.16
	STD	0.03	0.02	0.06	0.05
	Median	0.22	0.17	0.28	0.17
	Max.	0.76	0.28	0.93	0.35
Rio Branco	Mean	0.25	0.18	0.32	0.19
	STD	0.11	0.02	0.18	0.03
	Median	0.22	0.17	0.27	0.18
	Max.	1.05	0.32	1.01	0.38
Santa Cruz	Mean	0.25	0.18	0.38	0.13
	STD	0.08	0.03	0.19	0.06
	Median	0.23	0.17	0.31	0.12
	Max.	0.97	0.28	1.17	0.39
La Paz	Mean	0.34	0.22	0.38	0.24
	STD	0.07	0.03	0.08	0.04
	Median	0.34	0.16	0.37	0.23
	Max.	1.14	0.35	1.08	0.51



homogeneity in the biomass-burning process with respect to particle size. The relatively large variability in the non biomass-burning season can be explained by the highly variable background aerosol conditions with mixtures of different aerosol types prevailing. The typically larger uncertainties in  $r_{\text{eff}}$  and  $r_{\text{fine}}$  for low aerosol loads can also explain some of the increased variability. The Santa Cruz station shows larger  $r_{\text{eff}}$  during the non biomass-burning season which, as noted before, could be associated with coarse particles transported from local riverbeds as described in association with Fig. 9.

The highlands show systematically larger values of  $r_{\text{eff}}$  and  $r_{\text{fine}}$  independently of the season. The slightly lower values of both parameters during the biomass-burning season can be explained by the transport of smoke particles which, as previously noted, are predominantly fine mode. Aging of the transported particles (e.g. Eck et al., 2003; O'Neill et al., 2008b) could explain the larger  $r_{\text{eff}}$  and  $r_{\text{fine}}$ . The permanent coarse mode associated with dust on the Altiplano could also have an influence in terms of an increase in  $r_{\text{eff}}$ . The wind regime in the high mountains can favour accumulation of particles and can explain the larger values of  $r_{\text{fine}}$  compared to the lowlands (Vuille, 1999).

The dependences of particle size on aerosol load is illustrated in Fig. 11 where we represent  $r_{\text{eff}}$  and  $r_{\text{fine}}$  versus the AOD at 500 nm for the combination of all lowland data. Again, Linear Estimation and O'Neill et al. (2005) are used for the retrievals of  $r_{\text{eff}}$  and  $r_{\text{fine}}$ , respectively. We constrained the data plotted to conditions of AOD > 1.0 in order to limit the study to smoke particles only. Higher temporal-resolution retrievals of  $r_{\text{eff}}$  and  $r_{\text{fine}}$  do provide larger

datasets and also do allow retrievals for very high AODs which may be affected by partly cloudy skies (see our argument above for the greater probability of clouds being associated with smoke aerosols).

Fig. 11 shows linear trends of  $r_{\text{eff}}$  and  $r_{\text{fine}}$  with AOD increases. Similar patterns were obtained by using the operational AERONET almucantar retrieval algorithm, although the lower number of data introduced more uncertainty in the linear regressions. Actually, maximum AODs for AERONET retrievals were for ~3.2, while for data of Fig. 11 that maximum is for ~6.0. Root-mean-square differences are ~0.027 for  $r_{\text{eff}}$  and ~0.016 for  $r_{\text{fine}}$ . The results of the linear fits shown in Fig. 11 indicate that  $r_{\text{fine}}$  is nominally more sensitive to changes in AOD (the slope of the regression line is larger). The difference, for example, between the minimum and maximum AOD values of 1.0 and 6.0 is 0.035  $\mu\text{m}$  for the associated  $r_{\text{eff}}$  regression line. This is small compared with the  $r_{\text{eff}}$  values. The analogous  $r_{\text{fine}}$  calculation (a regression line increase of 0.065  $\mu\text{m}$  for the same range of AODs), corresponds to a change of approximately 40%. Such large aerosol loads favour the accumulation of particles in the atmosphere and, can therefore favor particle aging. For example, larger  $r_{\text{fine}}$  and  $r_{\text{eff}}$  have been found during the night due mainly to particle accumulations (e.g. Pérez-Ramírez et al., 2012). Also, coagulation rates increase as particle concentration (or AOD) increases (Colarco et al., 2003). The observed trend of increasing fine mode particle size in Amazonia as AOD increases is consistent with the findings of Schafer et al. (2008) from AERONET almucantar retrievals.

#### 3.4. Aerosol single scattering albedo, refractive index and asymmetry factor

For primary (directly retrieved) optical parameters such as the refractive index and derived optical parameters such as the single scattering albedo (SSA) the only source of information in this study is the AERONET almucantar scan/extinction spectrum retrieval. Level 2.0 data, the most reliable inversion product, is constrained by several quality control criteria (see Holben et al., 2006 for more details on the Level 2.0, Version 2.0 inversion criteria). Also, for intensive parameters such as SSA, asymmetry factor and refractive index, the retrieval uncertainties increase rapidly with decreasing AOD: this type of dependence was the motivation behind the Level 2.0 criterion that limits retrievals of these parameters to conditions where AOD(440 nm) > 0.4 (Holben et al., 2006). Because of this AOD > 0.4 requirement, Level 2.0 La Paz data over the whole database were limited to just six retrievals acquired during the 21st to 25th September 2010 period. Thus for this station only, we used Level 1.5 data that fulfilled the Level 2.0 sky conditions - sky errors, solar zenith scattering angle criterion - while constraining the retrievals to AOD values > 0.2. The analyses are only done for the biomass-burning seasons since there are little retrievals during the other seasons. The main statistical parameters of SSA, real and imaginary refractive index and asymmetry factor are listed in Table 4 (for a wavelength at 500 nm from linear interpolation of values at 440 and 670 nm).

From Table 4, SSA is generally lower in the highlands, implying more absorbing particles. The imaginary part of the refractive index exhibits considerably larger values in the highlands (i.e. stronger absorption with imaginary refractive index values that are, except for Cuiba, greater by ~0.005 than the lowland cases). The real part of the refractive index is approximately the same for the different lowland stations, while the highland station values are significantly higher. Finally, there are differences in the asymmetry factor, mostly in the near infrared region, that are likely related to particle size differences. The changes between the lowland and highland retrieval parameters of Table 4 suggest changes in particle composition (notably the real part of the refractive index).

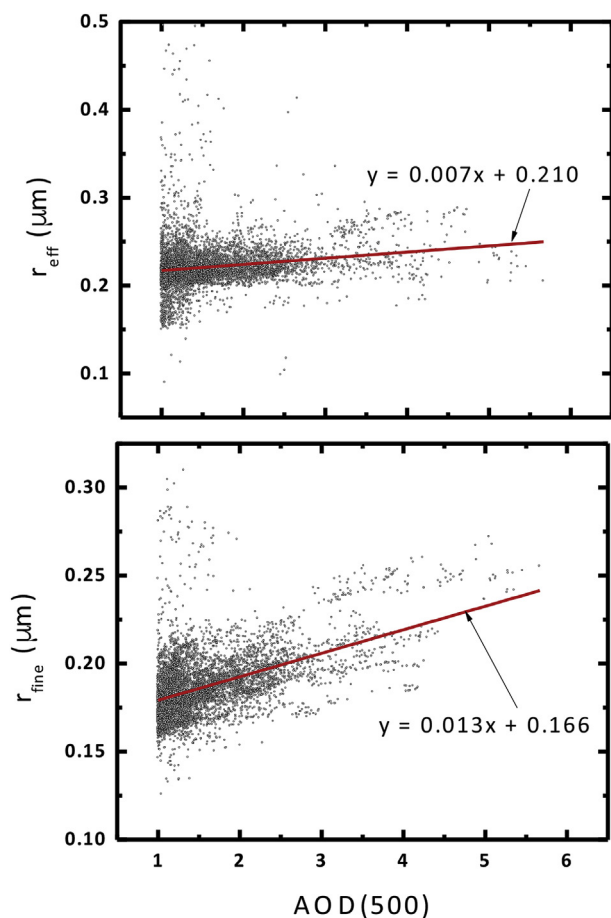


Fig. 11. Effective radius ( $r_{\text{eff}}$ ) and effective radius of the fine mode ( $r_{\text{fine}}$ ) versus aerosol optical depth (AOD) at 500 nm for the lowland data. Data selected are for AOD > 1.0.

**Table 4**  
Mean, standard deviation (STD), median and maximum (Max.) and minimum (Min.) values of aerosol single scattering albedo (SSA), asymmetry factor ( $g$ ) and real ( $m_r$ ) and imaginary ( $m_i$ ) part of refractive index. Data are presented only for biomass-burning data as most of the data that fulfill AERONET requirements are acquired in this season. These values are the result of linearly interpolating retrieval values at 440–670 to 500 nm. Data in brackets represent the number of retrievals for each place.

		SSA	$g$	$m_r$	$m_i$
Cuiaba <554>	Mean	0.88	0.65	1.46	0.019
	STD	0.05	0.02	0.06	0.010
	Median	0.88	0.65	1.47	0.017
	Max.	1.00	0.72	1.6	0.060
	Min.	0.71	0.59	1.34	0.001
Ji Parana <492>	Mean	0.92	0.65	1.48	0.011
	STD	0.02	0.02	0.05	0.004
	Median	0.93	0.65	1.48	0.011
	Max.	0.99	0.73	1.60	0.027
	Min.	0.84	0.59	1.34	0.001
Rio Branco <425>	Mean	0.91	0.66	1.47	0.015
	STD	0.04	0.02	0.05	0.007
	Median	0.92	0.73	1.47	0.013
	Max.	1.00	0.66	1.60	0.044
	Min.	0.79	0.60	1.34	0.001
Santa Cruz <158>	Mean	0.91	0.67	1.48	0.015
	STD	0.04	0.02	0.05	0.010
	Median	0.93	0.67	1.48	0.011
	Max.	0.98	0.71	1.60	0.065
	Min.	0.73	0.61	1.34	0.003
La Paz <36>	Mean	0.87	0.68	1.50	0.016
	STD	0.04	0.02	0.07	0.007
	Median	0.87	0.69	1.50	0.015
	Max.	0.93	0.72	1.60	0.036
	Min.	0.78	0.61	1.35	0.007

Larger SSA values being associated with the long-range transport of biomass-burning particles is known in the literature (e.g. Colarco et al., 2004). In the case of inter-regional transport between the lowlands and the highlands, the explanation of the differences in particle composition is hypothesized to be the large differences in the availability of water vapor in the atmosphere commented before: hygroscopic particles grow quickly by humidification in the lowlands (see, for e.g. Kotchenruther and Hobbs, 1998 and Kreidenweis et al., 2001 for general discussions on humidity induced particle growth of smoke particles). The water vapor condenses on the particles making them larger thereby increasing their scattering efficiency while also decreasing their imaginary refractive index, resulting in making them less absorbing. At higher altitudes, this particle growth effect is less probable due to the less availability of water vapor as well as the fact that the water coatings of particles uplifted from the lowlands may have largely evaporated. In spite of the possible mixture of smoke with local particles, the lower values of the real part of refractive index in the lowlands ( $\sim 1.47$ ) versus the highlands ( $\sim 1.53$ ) would support a hypothesis of humidification. It must however be borne in mind that, although humidification of biomass-burning particles affects their properties in general, our retrievals involve column-integrated properties, and we must accordingly be careful to not infer more from those retrievals than can be justified. Indeed, these limitations indicate that more investigations into smoke dynamics are needed than we carried out in our study. In particular, experimental plans would need to include resources for the measurement of vertical-profiles of aerosol properties such as those performed in the SAFARI-2000 field campaign (Swap et al., 2003), either by airplanes (Hobbs et al., 2003) or lidar measurements (McGill et al., 2003; Veselovskii et al., 2009).

Because SSA is a key aerosol radiative forcing parameter, it is important to study both its spatial and temporal evolution. To that end, Fig. 12 shows the mean SSA and AOD means at 500 nm (computed from linear interpolation using 440 and 675 nm values) for the lowland stations and for each biomass-burning season during the 2000–2013 period. The year to year averages of Fig. 12a

reflect the influence of the day-to-day variations of Fig. 2 with, for example, peaks in 2005, 2006, 2007 and 2010 (except that the mean values of Fig. 12a seem larger than expected: this is because the inversion processing protocols exclude retrievals for which AOD(440) is less than 0.4). With respect to the SSA, we note significant station-to-station variability in Fig. 12b. The SSA analysis reveals curious results: for the large AOD years (2005, 2006, 2007 and 2010) the values of SSA are approximately similar among the stations with an average that is close to 0.90. However, for the years of lower AODs (e.g. 2003, 2004 and 2008), SSA values are lower (0.85–0.78) at Cuiaba and Santa Cruz, while at Rio Branco and Ji Parana the values remain around 0.92. During the years of very intense burning activity (2005, 2006, 2007 and 2010) the burned area is very extensive in area: there is accordingly an enormous loading of particles in the atmosphere that arguably produce spatial homogenization of aerosol properties associated with greater regional transport dynamics. For smaller AODs the aerosols are not so regionally homogenous and differences in particle properties can arise between different sites. During low biomass-burning years at the southern Cuiaba and Santa Cruz sites, cerrado and agricultural burning is very likely more dominant. During higher biomass-burning years there would be more long-range transport of higher AOD plumes from the forest burning regions towards the south and west (Freitas et al., 2005). The cerrado vegetation (savannah type) burns with relatively more flaming phase combustion, thereby producing more black carbon. This results in lower SSA than smoke from forest burning regions which have a higher percentage of smoldering phase combustion from woody fuels therefore producing less black carbon (e.g. Ward et al., 1992; Reid et al., 2005a,b).

A scatterplot analysis of SSA versus AOD is shown in Fig. 13. The large SSA values of approximately 0.90–0.95 for very large AOD values are observed again for all the stations. For lower AODs there are, as discussed above, site-dependences with low SSA values in Cuiaba and Santa Cruz and larger values in Ji Parana and Rio Branco. Lower AOD with low SSA is particularly observed in 2008, when an anomaly in the biomass-burning pattern was observed using OMI

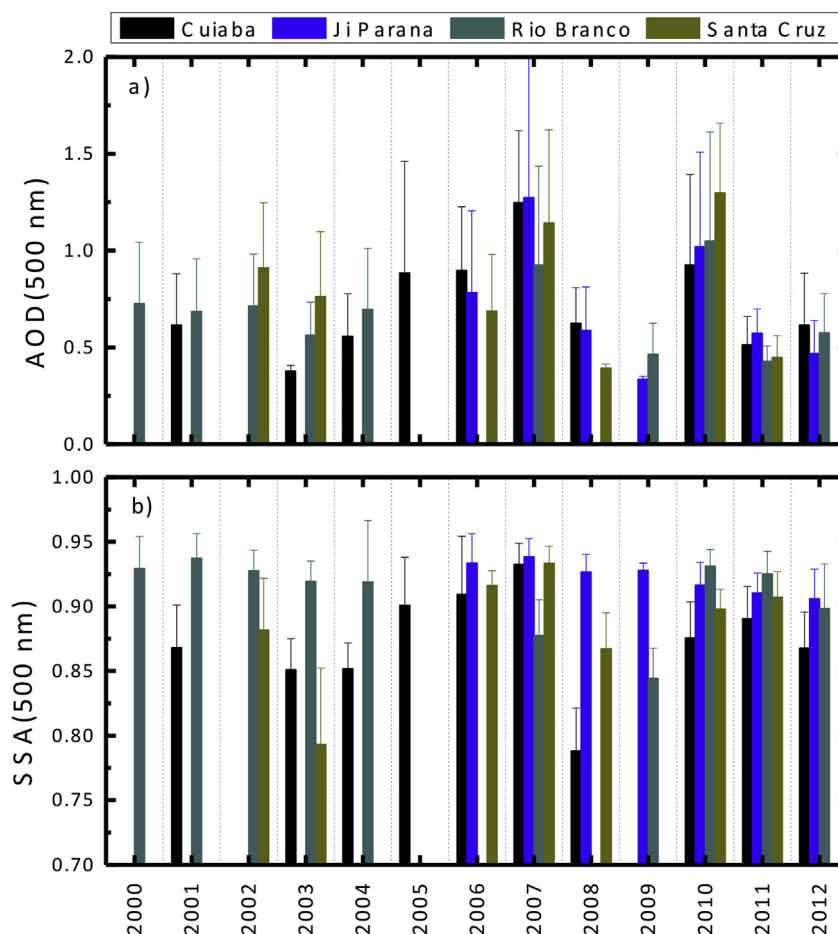


**Fig. 12.** Temporal evolution of the means and standard deviations of (a) aerosol optical depth (AOD) and (b) single scattering albedos (SSA) during the biomass-burning seasons for the lowland. Reference wavelength is at 500 nm.

data (Torres et al., 2010). For that year we note the rather extraordinary AERONET station-to-station SSA differences (which the OMI sensor, with its coarse spatial resolution of  $1^\circ \times 1^\circ$ , is largely insensitive to). The fact that the fires were less intense and sparser, and/or that particle-type emission differences occurred between

the savannah-like cerrado vegetation and the rainforest, could explain the lack of SSA spatial homogeneity.

### 3.5. Aerosol transport patterns to the highlands: biomass-burning case study in September–October 2010

Our goal in this section is to illustrate the smoke patterns and transport from the lowlands to the highlands during one carefully analysed biomass-burning season. We particularly investigated the intense biomass-burning season of September–October 2010 when large AODs (0.5) were registered at La Paz on a few days. Such AODs values are more than three times the average at La Paz. Fig. 14 shows the temporal evolution of AOD,  $\alpha(440-870)$ ,  $r_{\text{eff}}$  and  $r_{\text{fine}}$  for this case study at the Cuiaba, Ji-Parana, Rio Branco, Santa Cruz and La Paz stations.

We divided the biomass-burning case study period into five sub-periods. The first subperiod (I) goes from 1 to 18 September and is characterized by strong biomass-burning in the lowlands with AODs of up to 3.2. The Angstrom parameters values of around 1.8 along with  $\eta > 0.9$  indicate a predominance of fine particles. In this period there were no measurements at the La Paz station until 15th September. However, AOD values at La Paz on this day are very low suggesting weak transport of biomass-particles to the Andean Altiplano. The MODIS image for September 17th (Fig. 15a) shows the smoke plume pushed toward the eastern regions (Cuiaba, Ji Parana and Santa Cruz), while the areas close to Rio Branco, the foothills and the highlands, look less turbid.

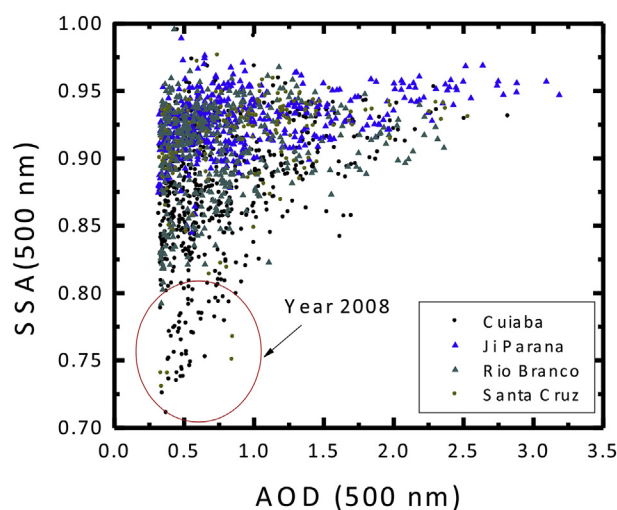


**Fig. 13.** Single scattering albedo (SSA) versus aerosol optical depth (AOD) for the complete AERONET Level 2.0 database in the lowlands.

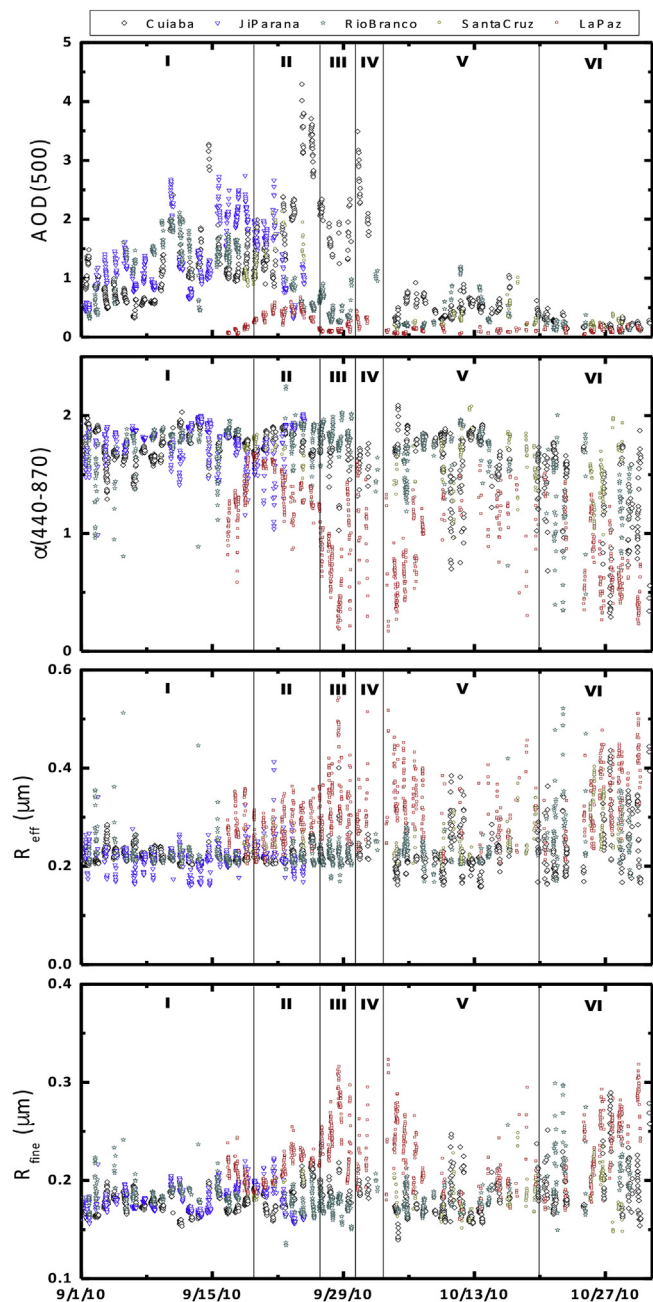


**Fig. 14.** Temporal evolution of aerosol optical at 500 nm (AOD), Angstrom parameter ( $\alpha(440-870)$ ), effective radius ( $r_{\text{eff}}$ ) and effective radius of the fine mode ( $r_{\text{fine}}$ ) for the period August–October 2010.

The second subperiod (II) from 18th to 25th September includes intense biomass-burning events that reach the La Paz region. Smoke plumes can be seen to be bordering the highlands in the MODIS image for 21st September (Fig. 15b). In this subperiod, the largest AODs of the entire database at La Paz were registered (up to 0.6), with a mean value of approximately 0.5. An increase in  $\alpha(440-870)$  associated with the arrival of fine mode biomass-burning particles is also evident in Fig. 14. The values of  $r_{\text{fine}}$  are relatively small ( $\sim 0.19 \mu\text{m}$ ), robust and stable (low scatter during this day). After the third day (21st September), the decrease of  $\alpha(440-870)$ , the increase of  $r_{\text{eff}}$  and the clear increase of  $r_{\text{fine}}$  suggest fine mode aerosol aging (maybe accompanied by the presence of some coarse mode). This could be explained, for example, by the

growth effects (such as coagulation) induced by the accumulation of smoke particles over several days (e.g. Reid et al., 2005a,b).

The study of air-mass transport to the highlands was initially done by computing backward trajectories using HYSPLIT. On 17th September air-masses arriving at 1500 m a.g.l. originated over the Pacific Ocean (the backward-trajectories are provided in the supplement) indicate prevailing westerly winds and explain the movement of the biomass plume towards the East compared to what was observed on previous days. For the intense biomass-burning on 21st September, the backward-trajectories arriving at 750 and 1500 m a.g.l. (graphs in the supplement) encounter the mountains producing an unrealistic calculation since the vertical velocities are essentially zero. The same is observed on 17 September for the 750 m a.g.l. backward-trajectory. To ameliorate this problem, HYSPLIT offers the possibility of coupling backward-trajectory calculations with a Lagrangian dispersion component (Stein et al., 2015). The use of air concentration backward-trajectories allows us to represent the uncertainty in the calculation arising from the model's characterization of the random motions created by atmospheric turbulence. The concentration pattern identifies the potential sources that might have contributed to the particles arriving at the site in question. Fig. 16 shows the air concentration of particles at La Paz station for integration periods of 5 days (120 h). Model initialization heights were 300 and 2000 m a.g.l. (approximately in and above the planetary boundary layer), with a total of 25,000 particles.

Fig. 16a and b show very similar patterns of the potential sources that could have influenced concentrations at the two representative heights of 300 and 2000 m a.g.l. on 17th September 2010. The largest concentrations are  $\sim 1\text{E-}13 \text{ units/m}^3$  in the area surrounding La Paz. Other potential sources are located in the North and Northeast regions and in the transit area between the highlands and lowlands (foothills that are locally known as 'Las Yungas'). The backward air concentration evaluated every 6 h (graphs shown in the supplement) reveal that air masses that started in the previous 1–2 days had their origin in the region close to La Paz while those further from the North and the Pacific Ocean are from the last 4–5 days. Such complex patterns of air concentration are associated with the westerly winds from the Pacific at high altitudes ( $>1500 \text{ m a.g.l.}$ ) and slow winds at low altitudes ( $<750 \text{ m a.g.l.}$ ).

Fig. 16c and d also show similar patterns for the two levels on 21st September 2010, with almost no particles transported from the west region while the largest potential sources are in the Amazonian lowlands to the east. Long-range transport is observed from the eastern regions of Bolivia and its border with Brazil, and even, for the 300 m a.g.l. level, from more distant areas in Brazil, northern Paraguay and Argentina. The backward air concentration evaluations for every 6 h (graphs shown in the supplement) reveal that the areas with lower concentrations correspond approximately to the previous 3–5 days while larger concentration areas correspond to the previous 1–3 days.

Fig. 17 shows CALIPSO lidar attenuated backscatter at 532 nm and vertical feature mask for 20th September 2010 when the instrument passed over South America close to the study region. The plot also shows the mean height above sea level. For the study region we observe intense attenuated backscatter that is classified by the feature mask algorithm (Omar et al., 2009) as tropospheric aerosol. According to our analyses of Figs. 15 and 16 such aerosol particles correspond to smoke particles. The attenuated backscatter values are close to that found in the literature for smoke particles in Amazonia (e.g. Baars et al., 2012). It is clearly seen that the mountains act as a natural barrier, with aerosol accumulating in the lowlands along the southern and northern sides of the Andes Mountains. It is also observed that smoke plumes can reach the high mountains, but with considerably lower amounts than in the



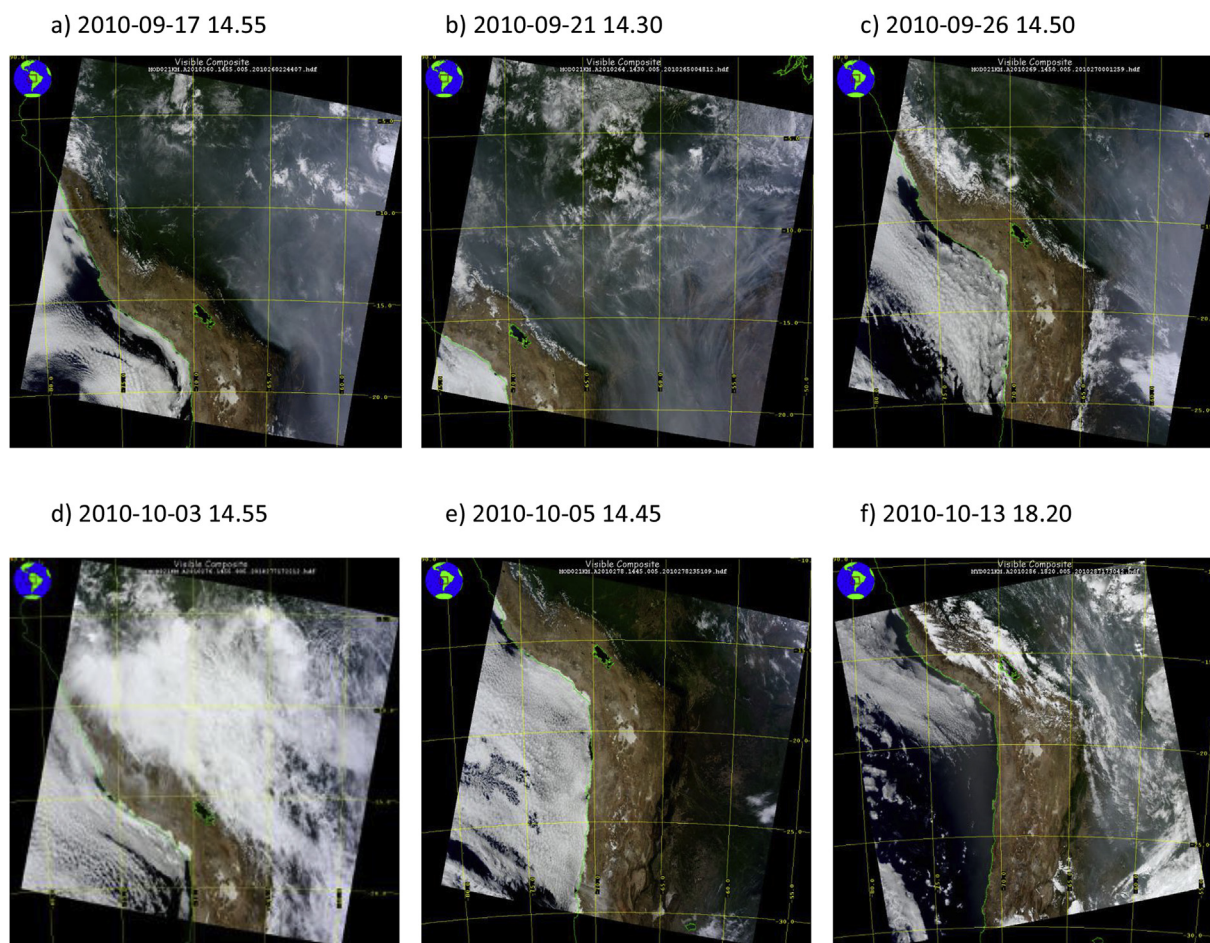


Fig. 15. MODIS images for (a) 17/09/2010 (b) 21/09/2010 (c) 26/09/2010 (d) 03/10/2010 (e) 05/10/2010 and (f) 13/10/2010.

lowlands. In fact, some of these plumes have AOD values close to the detection limit of CALIPSO. All these findings agree with our general analyses of smoke particles transported to Andean high mountains. Unfortunately, CALIPSO did not cross over La Paz during the days of interest to this study and no direct comparison with this station could be done.

The third subperiod (III) from 26th to 29th September is also characterized by air-masses with origins in the Pacific Ocean (backward-trajectories not shown). Very low AODs were registered again in Rio Branco and La Paz (the western locations) and the MODIS image (Fig. 15c) shows that the smoke particles have apparently moved toward the east relative to the MODIS image of Fig. 15b. These findings again support the notion that strong westerly winds cleaned the atmosphere. Large highland variability in  $\alpha(440-870)$ ,  $r_{\text{eff}}$  and  $r_{\text{fine}}$ , associated with large uncertainties for low aerosol loads, is observed again. The presence of coarse mode particles at the highland station is again inferred from smaller values of  $\alpha(440-870)$  and larger values of  $r_{\text{eff}}$ . The situation is however different to the East as indicated by the large AODs in Cuiba.

The fourth subperiod (IV) extends from 30th September to 3rd October and is characterized by a change of the air-mass origin towards the northeast in the vicinity of Peru. For this case backward-trajectories (graphs included in the supplement) are not adversely affected by the high mountains as they were for the other dates. During this period the most relevant factor is the significant amount of cloud cover (as observed in the MODIS image of Fig. 15d)

both in the Pacific and in the Amazonia basin.

The last subperiods (V & VI) of Fig. 14 extends from 3rd to 31st October and was generally characterized by the two different air-mass patterns identified above. In this subperiod we note the considerably lower aerosol load at all the stations compared to the values registered in September. In general the atmosphere was clean during this subperiod as illustrated by the MODIS image on the 5th of October (Fig. 15e). For this day, air-masses encountered the mountains and the backward dispersion air concentrations were again employed (see graphs in the supplement), with patterns similar to these of Fig. 16a and b and particles originating from the northwest and southwest highlands and the Pacific Ocean. Therefore, no transport of biomass-burning to La Paz was expected on October 5th, which is consistent with the weak AODs of Fig. 14 and the MODIS image (Fig. 15e). On the other hand, between 10th and 15th October were registered sparse lowland biomass-burning events with some AODs above 0.4, high values of  $\alpha(440-870)$  (close to 1.8) and stable values of  $r_{\text{eff}}$  and  $r_{\text{fine}}$  of 0.22 and 0.19  $\mu\text{m}$ . The MODIS Aqua image for October 13th (Fig. 15f) supports the characterization of “sparse” and shows more intense and homogeneous biomass-burning plumes to the east of La Paz. Air concentration backward-trajectory analyses were again required: the long-range transport from the lowlands in the Amazon is similar to that observed for the intense smoke events of the 20th September at La Paz (see graphs in the supplement). In this case, however, no important AOD enhancement was registered at the La Paz station. The main reason for this is likely the sparse (and

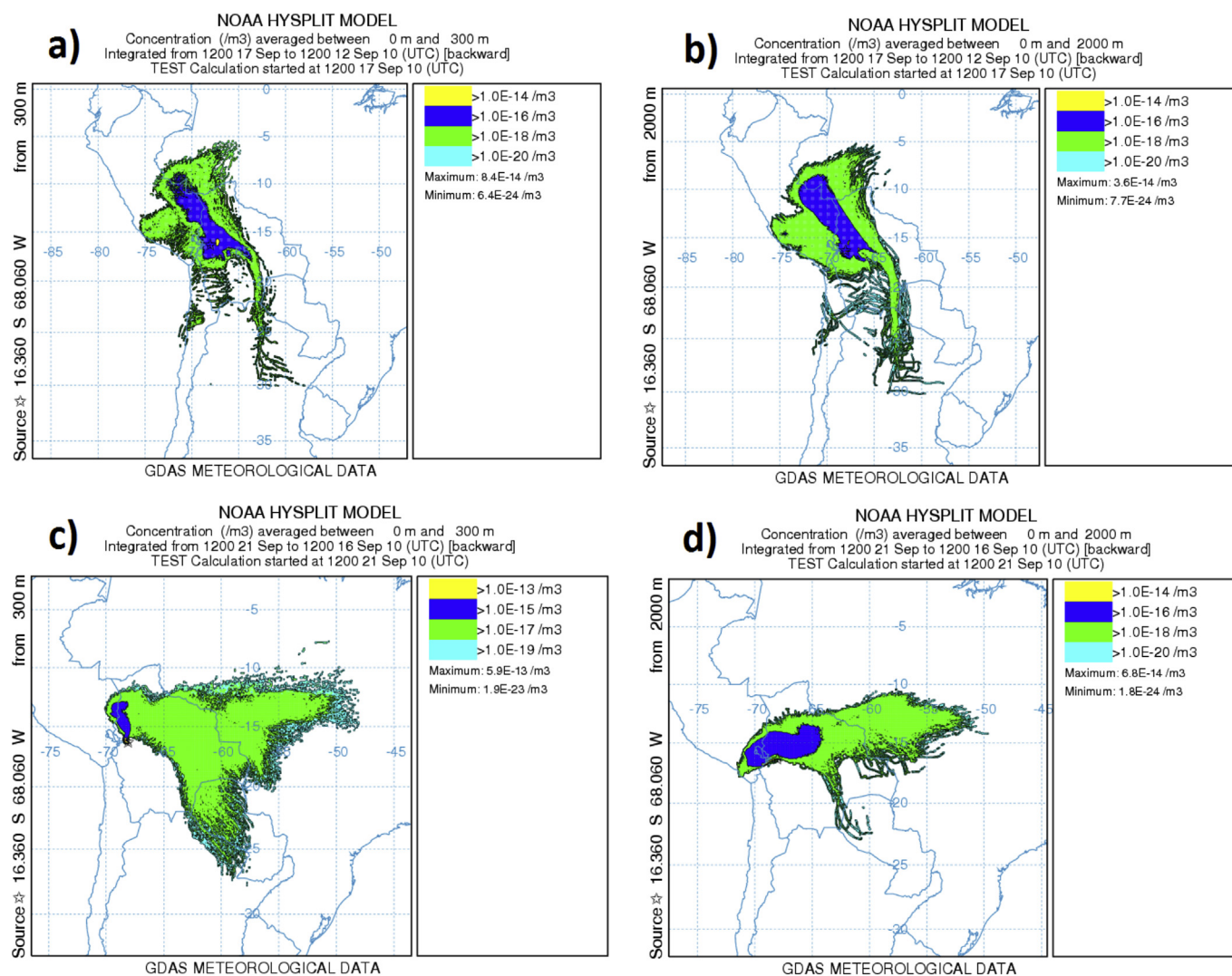


**Fig. 16.** Air concentration backward dispersion for the city of La Paz for 17/09/2010 and 21/09/2010 for two altitude intervals: 0–300 m a.g.l. (left hand plots) and 0–2000 m a.g.l. (right hand plots). La Paz is identified by the tiny black empty star.

probably low intensity) nature of fires in the lowlands during the 10th–15th October period.

An analysis of wind regimes over La Paz for the August–October 2010 period reveals that, at the 750 and 1500 m a.g.l. levels, 16–22% of the cases were associated with westerly winds, while the rest (percentages around 80%) were associated with easterly winds originated in the lowlands at the Amazonia. Although the analyses were for the particular biomass-burning season of 2010, the results may be representative of the general patterns that favour/suppress the transport of smoke particles in the tropical Andean region. More in depth studies would require the use of very high temporal-resolution meteorological data, and a large dataset of meteorological variable measurements for a more comprehensive evaluation of these patterns. Profile analyses using active remote sensing measurements are also required (e.g. multiwavelength lidar) to better understand the vertical profile of the transported smoke particles.

#### 4. Conclusions

We carried out an analysis of columnar aerosol properties in the South American tropical region within 10–20° South and 50–70° West. The area includes the Amazon (lowlands), the high mountain

regions (highlands) and the transition between the two (foothills). Precipitation in the region occurs mainly in the December–March period while the June–October period is very dry. The most important geo-atmospheric factor is the strong altitude gradient between the lowlands and the highlands, which implies change in vegetation and in water vapor concentration. The contrast of aerosol properties between the lowlands and highlands is studied using the 2000–2014 AERONET measurements across the lowland stations of Rio Branco, Ji Parana, Cuiaba (stations in Brazil) and Santa Cruz (Bolivia) and the highlands station of La Paz (Bolivia).

For the lowlands, an enhanced annual cycle in aerosol optical depth (AODs) and Angstrom parameter ( $\alpha(440-870)$ ) was observed during the biomass-burning season (August–October) across all the stations. Year to year variability, with maximum AODs in 2005, 2006, 2007 and 2010 was observed and directly linked to biomass burning activity. Using TRMM satellite data, precipitation links were studied within the context of precipitation anomalies defined as the difference between annual and climatological values for the wet (November–March) dry (April–July) and biomass-burning (August–October) seasons. Positive anomalies during the wet season influence the amount of vegetation available to be burned, while negative anomalies in the dry period favours fire



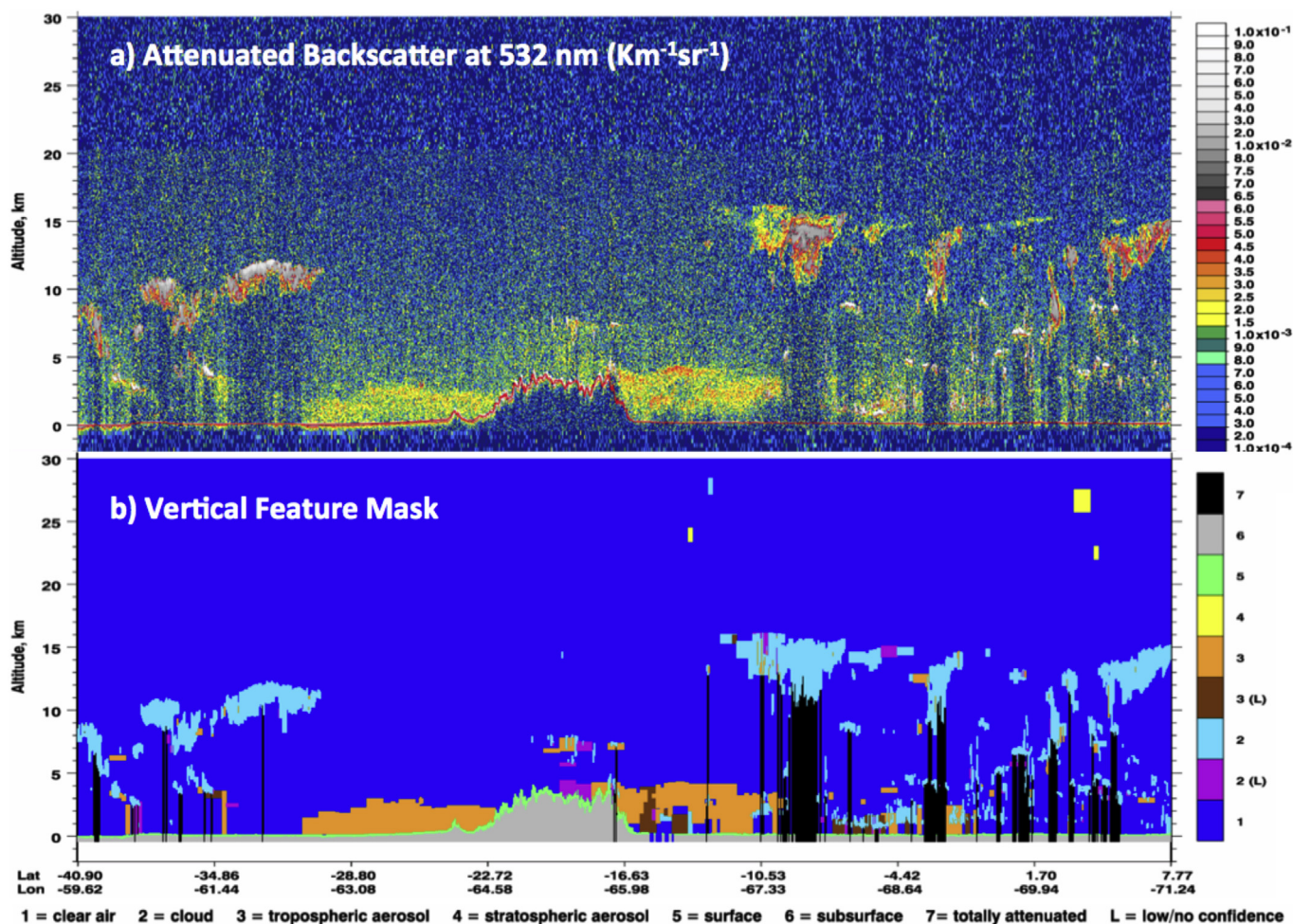


**Fig. 17.** Attenuated backscatter and vertical feature mask for CALIPSO data acquired on 20th September 2010 over South America. Data were acquired between 18:11:49 and 18:25:18 UTC.

activity. This hypothesis was found for the intense biomass-burning seasons in 2005, 2006, 2007 and 2010, while the opposite happens in 2009 with lower fire activity. After 2010, however, we did not observe such links with precipitation. Other factors, such as the influence of government policies on burning practices could have had an impact on our proposed relationship between rainfall anomaly and AOD and thus future investigations are needed.

The analyses during the biomass-burning season in the lowlands showed, as expected, a large predominance of fine mode particles. We also demonstrated an increase, predominantly in the fine mode, of particle radius, as AOD increases. This demonstration was achieved because we used the much more numerous retrievals of particle radius from spectral AOD measurements in spite of the larger uncertainties compared to AERONET standard retrievals. Such a finding is likely associated with the accumulation of particles. The study of the single scattering albedo (SSA) also revealed interesting findings: for the years of intense biomass-burning activity, values of SSA ( $\sim 0.93$ ) are homogeneous with very similar values among all the stations. However, for the years with less intense activity, such as 2008, intra-lowland differences arise with the SSA being larger ( $\sim 0.95$ ) at the northern stations of Rio Branco and Ji Parana and lower at the southern stations of Cuiaba and Santa Cruz (SSA values with mean of  $\sim 0.85$  and minimum values even below 0.75). In the northern locations, the biomass burning of the rainforest predominates while in the

other locations cerrado and agricultural burning is more dominant. The type of vegetation/rainforest burned could explain some of the differences observed in SSA. More investigation is needed to confirm or reject this hypothesis.

The La Paz highlands data also showed an annual AOD cycle with maximums during the biomass-burning season. These maximum values, ranging up to 0.5, are high for this region where the mean AOD is approximately 0.12. Ongoing studies with in-situ instrumentation are revealing the presence of anthropogenic particles during the whole year, and the only sources in the Bolivian Altiplano of such particles are the local industry and road traffic in the La Paz region. Also, the natural sources of highland aerosols are associated with dust from the Altiplano, which is present during the whole year. Therefore, the seasonal enhancement of AOD is associated with the transport of lowland smoke. However, it was found that this transport is sporadic in nature. Highland particle radii showed important differences compared to lowland values: For the effective radius ( $r_{\text{eff}}$ ), which is sensitive to fine and coarse particles, systematically larger La Paz values were likely influenced by the continuous presence of dust particles from the Altiplano. The lowland station of Santa Cruz has shown the presence of coarse particles which we suggested was associated with wind-driven river bed erosion. Systematically larger values of fine mode radius ( $r_{\text{fine}}$ ) were observed at La Paz over the whole year. Because changes in  $r_{\text{fine}}$  are attributable to changes in the fine mode, these

differences were thought to be due to fine mode particle aging, a mechanism that is probably favoured by the high mountain wind regimes. Transport of smoke particles to the highlands was associated with larger highland values of particle size (both  $r_{\text{fine}}$  and  $r_{\text{eff}}$  were larger) whose growth was attributed to particle aging.

The transported smoke particles to the highlands had lower values of SSA: large relative (and specific) humidity in the lowlands favours particle growth by hygroscopicity with an attendant decrease in optical absorption. In the highlands, however, relative (and specific) humidity is quite low and it is likely that water, previously absorbed by the particles, evaporates. The SSA retrieval numbers are, however, relatively small and it has not been possible to verify this hypothesis. Comprehensive field campaigns will be needed to further identify the impact of transported biomass-burning particles, preferably including simultaneous lowland and highland measurements. These kinds of investigations are desired as future activities of the Global Atmospheric Watch activities focussed on the station at Mount Chacaltaya (5240 m a.s.l.) in Bolivia.

The analyses of the air-masses reaching the station of La Paz were carried out using the HYSPLIT model. It has been found that the computed flow of backward-trajectories frequently encounters mountains, thus introducing large uncertainties in the backward-trajectory computations. Indeed, the HYSPLIT air concentration backward-dispersion has been used to identify the potential sources that might have contributed to the particles arriving at the site in question. The analyses of air concentration backward-dispersion have revealed that easterly winds predominate allow the transport of biomass-burning particles from the Amazonian lowlands, including regions of eastern Brazil, northern Paraguay and northern Argentina to the highlands. On the other hand, westerly winds help to clean the atmosphere. HYSPLIT allow being coupled with mesoscale models such as the Weather and Research Forecast (WRF) model, and that will allow the identification of detailed transport of pollutants through the mountains. Such advances are necessary for better understanding the vulnerability of the Andean high mountain regions to climate change. These climate-driven studies must be combined with others in glaciology to study water resources, water quality and water use efficiency, and will support environmental and economic development of the nations of the Andean regions.

## Acknowledgments

This work was supported by the Marie Skłodowska-Curie Individual Fellowships (IF) ACE\_GFAT (grant agreement No 659398), by the Postdoctoral Program of the University of Granada (Program 8), by the NASA Atmospheric Composition Program and by the NASA Aerosols, Clouds, Ecosystems mission. The work was also supported by the Andalusia Regional Government through project P12-RNM-2409 by the Spanish Ministry of Economy and Competitiveness and FEDER through project CGL2013-45410-R and CGL2016-81092-R, and by European Union's Horizon 2020 Research and Innovation Programme under grant agreement No. 654109, ACTRIS-2. The authors thankfully acknowledge the AERONET team for maintaining the stations used in this work and to the NOAA Air Research Laboratory for providing the HYSPLIT model.

## Appendix A. Supplementary data

Supplementary data related to this article can be found at <http://dx.doi.org/10.1016/j.atmosenv.2017.07.037>.

## References

- Alados-Arboledas, L., Müller, D., Guerrero-Rascado, J.L., Navas-Guzmán, F., Pérez-Ramírez, D., Olmo, F.J., 2011. Optical and microphysical properties of fresh biomass burning aerosol retrieved by Raman lidar, and star-and-sun-photometry. *Geophys. Res. Lett.* 38.
- Alastuey, A., 2017. Measurements of PM10 and PM2.5 at the Bolivian Andean Altiplano and in La Paz Region. Personal Communication, Chacaltaya GAW Station Scientific Steering Committee, 7 June 2017, La Paz, Bolivia.
- Andreae, M.O., Merlet, P., 2001. Emission of trace gases and aerosols from biomass burning. *Glob. Biogeochem. Cycles* 15, 955–966.
- Baars, H., Ansmann, A., Althausen, D., Engelmann, R., Heese, B., Müller, D., Artaxo, P., Paixao, M., Pauliquevis, T., Souza, R., 2012. Aerosol profiling with lidar in the Amazon Basin during the wet and dry season. *J. Geophys. Res. Atmos.* 117 n/a–n/a.
- Bonasoni, P., Laj, P., Marinoni, A., Sprenger, M., Angelini, F., Arduini, J., Bonafé, U., Calzolari, F., Colombo, T., Decesari, S., Di Biagio, C., di Sarra, A.G., Evangelisti, F., Duchi, R., Facchini, M.C., Fuzzi, S., Gobbi, G.P., Maione, M., Panday, A., Roccato, F., Sellegri, K., Venzac, H., Verza, G.P., Villani, P., Vuilleumoz, E., Cristofanelli, P., 2010. Atmospheric brown clouds in the Himalayas: first two years of continuous observations at the Nepal climate observatory-pyramid (5079 m). *Atmos. Chem. Phys.* 10, 7515–7531.
- Bond, T.C., Doherty, S.J., Fahey, D.W., Forster, P.M., Bernsten, T., DeAngelo, B.J., Flanner, M.G., Ghan, S., Kärcher, B., Koch, D., Kinne, S., Kondo, Y., Quinn, P.K., Sorooshian, M.C., Schultz, M.G., Schulz, M., Venkataraman, C., Zhang, H., Zhang, S., Bellouin, N., Guttikunda, S.K., Hopke, P.K., Jacobson, M.Z., Kaiser, J.W., Klimont, Z., Lohmann, U., Schwarz, J.P., Shindell, D., Storelvmo, T., Warren, S.G., Zender, C.S., 2013. Bounding the role of black carbon in the climate system: a scientific assessment. *J. Geophys. Res. Atmos.* 118, 5380–5552.
- Boucher, E.H., Stein, A.F., 2016. Large salt dust storms follow a 30-year rainfall cycle in the Mar Chiquita Lake (Córdoba, Argentina). *PLoS One* 11 (6), e0156672 doi: 10.1371/journal.pone.0156672.
- Bourgeois, Q., Ekman, A.M.L., Krejci, R., 2015. Aerosol transport over the Andes from the Amazon Basin to the remote Pacific Ocean: a multiyear CALIOP assessment. *J. Geophys. Res. Atmos.* 120, 8411–8425.
- Bowman, D.M.J.S., Balch, J.K., Artaxo, P., Bond, W.J., Carlson, J.M., Cochrane, M.A., D'Antonio, C.M., DeFries, R.S., Doyle, J.C., Harrison, S.P., Johnston, F.H., Keeley, J.E., Krawchuk, M.A., Kull, A.C., Marston, J.B., Moritz, M.A., Prentice, I.C., Roos, C.I., Scott, A.C., Swetnam, T.W., van der Werf, G.R., Pyne, S.J., 2009. Fire in the Earth system. *Science* 324, 481–484.
- Bowman, D.M.J.S., Johnston, F.H., 2005. Wildfire smoke, fire management, and human health. *EcoHealth* 2, 76–80.
- Colarco, P.R., Toon, O.B., Holben, B.N., 2003. Saharan dust transport to the Caribbean during PRIDE: 1. Influence of dust sources and removal mechanisms on the timing and magnitude of downwind aerosol optical depth events from simulations of in situ and remote sensing observations. *J. Geophys. Res.* 108, 8589.
- Colarco, P.R., Schoeberl, M.R., Doddridge, B.G., Marufu, L.T., Torres, O., Welton, E.J., 2004. Transport of smoke from Canadian forest fires to the surface near Washington, D.C.: injection height, entrainment, and optical properties. *J. Geophys. Res.* 109.
- Crusius, J., Schroth, A.W., Gassó, S., Moy, C.M., Levy, R.C., Gatica, M., 2011. Glacial flour dust storms in the Gulf of Alaska: hydrologic and meteorological controls and their importance as a source of bioavailable iron. *Geophys. Res. Lett.* 38, L06602.
- Dubovik, O., King, M.D., 2000. A flexible inversion algorithm for retrieval of aerosol optical properties from Sun and sky radiance measurements. *J. Geophys. Res.* 105, 20673–20696.
- Dubovik, O., Holben, B.N., Eck, T.F., Smirnov, A., Kaufman, Y.J., King, M.D., Tanre, D., Slutsker, I., 2002. Variability of absorption and optical properties of key aerosol types observed in worldwide locations. *J. Atmos. Sci.* 59, 590–608.
- Dubovik, O., Sinyuk, A., Lapyonok, T., Holben, B.N., Mishchenko, M., Yang, P., Eck, T.F., Volten, H., Muñoz, O., Veihelmann, B., van der Zande, W.J., Leon, J.-F., Sorokin, M., Slutsker, I., 2006. Application of spheroid models to account for aerosol particle nonsphericity in remote sensing of desert dust. *J. Geophys. Res.* 111, D11208.
- Dumka, U.C., Moorthy, K.K., Satheesh, S.K., Sagar, R., Pant, P., 2008. Short-period modulations in aerosol optical depths over the central Himalayas: role of mesoscale processes. *J. Appl. Meteorology Climatol.* 47, 1467–1475.
- Eck, T.F., Holben, B.N., Reid, J.S., Dubovik, O., Smirnov, A., O'Neill, N.T., Slutsker, I., Kinne, S., 1999. Wavelength dependence of the optical depth of biomass burning, urban, and desert dust aerosols. *J. Geophys. Res.* 104, 31333–31349.
- Eck, T.F., Holben, B.N., Ward, D.E., Mukelabai, M.M., Dubovik, O., Smirnov, A., Schafer, J.S., Hsu, N.C., Piketh, S.J., Queface, A., Le Roux, J., Swap, R.J., Slutsker, I., 2003. Variability of biomass burning aerosol optical characteristics in southern Africa during the SAFARI 2000 dry season campaign and a comparison of single scattering albedo estimates from radiometric measurements. *J. Geophys. Res.* 108.
- Eck, T.F., Holben, B.N., Reid, J.S., Sinyuk, A., Hyer, E.J., O'Neill, N.T., Shaw, G.E., Vande Castle, J.R., Chapin, F.S., Dubovik, O., Smirnov, A., Vermote, E., Schafer, J.S., Giles, D., Slutsker, I., Sorokin, M., Newcomb, W.W., 2009. Optical properties of boreal region biomass burning aerosols in central Alaska and seasonal variation of aerosol optical depth at an Arctic coastal site. *J. Geophys. Res.* 114.
- Eck, T.F., Holben, B.N., Sinyuk, A., Pinker, R.T., Goloub, P., Chen, H., Chatenet, B., Li, Z., Singh, R.P., Tripathi, S.N., Reid, J.S., Giles, D.M., Dubovik, O., O'Neill, N.T.,



- Smirnov, A., Wang, P., Xia, X., 2010. Climatological aspects of the optical properties of fine/coarse mode aerosol mixtures. *J. Geophys. Res.* 115, D19205.
- Eck, T.F., Holben, B.N., Reid, J.S., Mukelabai, M.M., Piketh, S.J., Torres, O., Jethva, H.T., Hyer, E.J., Ward, D.E., Dubovik, O., Sinyuk, A., Schafer, J.S., Giles, D.M., Sorokin, M., Smirnov, A., Slutsker, I., 2013. A seasonal trend of single scattering albedo in southern African biomass-burning particles: implications for satellite products and estimates of emissions for the world's largest biomass-burning source. *J. Geophys. Res. Atmos.* 118, 6414–6432.
- Eck, T., Holben, B., Giles, D., Smirnov, A., Slutsker, I., Sinyuk, A., Schafer, J., Sorokin, M., Reid, J., Sayer, A., Hsu, C., Levy, R., Lyapustin, A., Wang, Y., Rahman, M.A., Liew, S.-C., Salinas Cortijo, S.V., Li, T., Kalbermatter, D., Keong, K.L., Elifant, M., Aditya, F., Mohamad, M., Chong, T.K., San, L.H., Choon, Y.E., Deranadayan, G., Kusumanigtyas, S., Mahmud, M., 2016. Remote sensing measurements of biomass burning aerosol optical properties during the 2015 Indonesian burning season from AERONET and MODIS satellite data. In: "Remote Sensing of Clouds and Aerosols: Techniques and Applications", European Geosciences Union General Assembly 2016, Vienna, Austria 17–22 April 2016. online available in: <http://meetingorganizer.copernicus.org/EGU2016/EGU2016-2391-3.pdf>.
- Freitas, S.R., Longo, K., Silva Dias, M.A.F., Silva Dias, P.L., Chatfield, R., Prins, E., Artaxo, P., Grell, G.A., Recuero, F.S., 2005. Monitoring the transport of biomass burning emissions in South America. *Environ. Fluid Mech.* 5, 135–167.
- Gaiero, D.M., Simonella, L., Gassó, S., Gili, S., Stein, A.F., Sosa, P., Becchio, R., Arce, J., Marelli, H., 2013. Ground/satellite observations and atmospheric modeling of dust storms originating in the high Puna-Altiplano deserts (South America): implications for the interpretation of paleo-climate archives. *J. Geophys. Res. Atmos.* 118, 3817–3831.
- Gautam, R., Hsu, N.C., Tsay, S.C., Lau, K.M., Holben, B., Bell, S., Smirnov, A., Li, C., Hansell, R., Ji, Q., Payra, S., Aryal, D., Kayastha, R., Kim, K.M., 2011. Accumulation of aerosols over the Indo-Gangetic plains and southern slopes of the Himalayas: distribution, properties and radiative effects during the 2009 pre-monsoon season. *Atmos. Chem. Phys.* 11, 12841–12863.
- Guirado, C., Cuevas, E., Cachorro, V.E., Toledano, C., Alonso-Pérez, S., Bustos, J.J., Basart, S., Romero, P.M., Camino, C., Mimouni, M., Zeudmi, L., Goloub, P., Baldasano, J.M., de Frutos, A.M., 2014. Aerosol characterization at the saharan AERONET site tamanrasset. *Atmos. Chem. Phys.* 14, 11753–11773.
- Hobbs, P.V., Sinha, P., Yokelson, R.J., Christian, T.J., Blake, D.R., Gao, S., Kirchstetter, T.W., Novakov, T., Pilewskie, P., 2003. Evolution of gases and particles from a savanna fire in South Africa. *J. Geophys. Res.* 108, 8485.
- Holben, B.N., Eck, T.F., Slutsker, I., Tanre, D., Buis, J.P., Setzer, A., Vermote, E., Reagan, J.A., Kaufman, Y.J., Nakajima, T., Lavenu, F., Jankowiak, I., Smirnov, A., 1998. AERONET- A federated instrument network and data archive for aerosol characterization. *Remote Sens. Environ.* 66, 1–16.
- Holben, B.N., Eck, T.F., Slutsker, I., Smirnov, A., Sinyuk, A., Schafer, J., Giles, D., Dubovik, O., 2006. Aeronet's Version 2.0 quality assurance criteria. *Proc. SPIE* 6408, 64080Q.
- Jacobson, M.Z., 2014. Effects of biomass burning on climate, accounting for heat and moisture fluxes, black and brown carbon, and cloud absorption effects. *J. Geophys. Res. Atmos.* 119, 8980–9002.
- Kim, D., Chin, M., Yu, H., Eck, T.F., Sinyuk, A., Smirnov, A., Holben, B.N., 2011. Dust optical properties over north Africa and Arabian Peninsula derived from the AERONET dataset. *Atmos. Chem. Phys.* 11, 10733–10741.
- Koren, I., Remer, L.A., Longo, K.M., 2007. Reversal of trend of biomass burning in the Amazon. *Geophys. Res. Lett.* 34, L20404.
- Koren, I., Martins, J.V., Remer, L.A., Afargan, H., 2008. Smoke invigoration versus inhibition of clouds over the Amazon. *Science* 321, 946–949.
- Koren, I., Remer, L.A., Longo, K., Brown, F., Lindsey, R., 2009. Reply to comment by W. Schroeder et al. on "Reversal of trend of biomass burning in the Amazon". *Geophys. Res. Lett.* 36, L03807.
- Kotchenruther, R.A., Hobbs, P.V., 1998. Humidification factors of aerosols from biomass burning in Brazil. *J. Geophys. Res.* 103, 32081–32089.
- Kreidenweis, S.M., Remer, L.A., Bruinjes, R., Dubovik, O., 2001. Smoke aerosol from biomass burning in Mexico: hygroscopic smoke optical model. *J. Geophys. Res.* 106, 4831–4844.
- Latrubesse, E.M., Stevaux, J.C., Cremon, E.H., May, J.-H., Tatum, S.H., Hurtado, M.A., Bezada, M., Argollo, J.B., 2012. Late quaternary megafans, fans and fluvio-aeolian interactions in the Bolivian Chaco, tropical south America. *Paleogeogr. Paleoclimatology, Palaeoecol.* 356–357, 75–88.
- Longo, K.M., Freitas, S.R., Andreae, M.O., Setzer, A., Prins, E., Artaxo, P., 2010. The coupled aerosol and tracer transport model to the Brazilian developments on the regional atmospheric modeling system (CAIT-BRAMS) – Part 2: model sensitivity to the biomass burning inventories. *Atmos. Chem. Phys.* 10, 5785–5795.
- Lüthi, Z.L., Skerlak, B., Kim, S.W., Lauer, A., Mues, A., Rupakheti, M., Kang, S., 2015. Atmospheric brown clouds reach the Tibetan Plateau by crossing the Himalayas. *Atmos. Chem. Phys.* 15, 6007–6021.
- Maione, M., Giostra, U., Arduini, J., Furlani, F., Bonasoni, P., Cristofanelli, P., Laj, P., Vuillemoz, E., 2011. Three-year observations of halocarbons at the Nepal Climate Observatory at Pyramid (NCO-P, 5079 m a.s.l.) on the Himalayan range. *Atmos. Chem. Phys.* 11, 3431–3441.
- Marq, S., Laj, P., Roger, J.C., Villani, P., Sellegri, K., Bonasoni, P., Marinoni, A., Cristofanelli, P., Verza, G.P., Bergin, M., 2010. Aerosol optical properties and radiative forcing in the high Himalaya based on measurements at the Nepal Climate Observatory-Pyramid site (5079 m a.s.l.). *Atmos. Chem. Phys.* 10, 5859–5872.
- Matichuk, R.I., Colarco, P.R., Smith, J.A., Toon, O.B., 2008. Modeling the transport and optical properties of smoke plumes from South American biomass burning. *J. Geophys. Res.* 113.
- McGill, M.J., Hlavka, D.L., Hart, W.D., Welton, E.J., Campbell, J.R., 2003. Airborne lidar measurements of aerosol optical properties during SAFARI-2000. *J. Geophys. Res.* 108, 8493.
- Mishra, A.K., Lehahn, Y., Rudich, Y., Koren, I., 2015. Co-variability of smoke and fire in the Amazon basin. *Atmos. Environ.* 109, 97–104.
- Morton, D.C., Defries, R.S., Randerson, J.T., Giglio, L., Schroeder, W., Van Der Werf, G.R., 2008. Agricultural intensification increases deforestation fire activity in Amazonia. *Glob. Change Biol.* 14, 2262–2275.
- Nogues-Paegle, J., Mo, K., 1997. Alternating Wet and Dry Conditions over South America during Summer. *Monthly Weather Review*, vol. 125.
- Noh, Y.M., Müller, D., Shin, D.H., Lee, H., Jung, J.S., Lee, K.H., Cribb, M., Li, Z., Kim, Y.J., 2009. Optical and microphysical properties of severe haze and smoke aerosol measured by integrated remote sensing techniques in Gwangju, Korea. *Atmos. Environ.* 43, 879–888.
- Omar, A.H., Winker, D.M., Kittaka, C., Vaughan, M.A., Liu, Z., Hu, Y., Hostetler, C.A., 2009. The CALIPSO automated aerosol classification and lidar ratio selection algorithm. *J. Atmos. Oceanic Techniques* 26, 1994–2014, 2009.
- O'Neill, N.T., Dubovik, O., Eck, T.F., 2001a. Applied Optics. Modified Angstrom Exponent for the Characterization of Submicrometer Aerosols, vol. 40, pp. 2368–2375.
- O'Neill, N.T., Eck, T.F., Holben, B.N., Smirnov, A., Dubovik, O., Royer, A., 2001b. Bimodal size distribution influences on the variation of Angstrom derivatives in spectral optical depth space. *J. Geophys. Res.* 106.
- O'Neill, N.T., Eck, T.F., Smirnov, A., Holben, B.N., Thulasiraman, S., 2003. Spectral discrimination of coarse and fine mode optical depth. *J. Geophys. Res.* 108.
- O'Neill, N.T., Thulasiraman, S., Eck, T.F., Reid, J.S., 2005. Robust optical features of fine mode size distributions: application to the Québec smoke event of 2002. *J. Geophys. Res.* 110, D011207.
- O'Neill, N.T., Thulasiraman, S., Eck, T.F., Reid, J.S., 2008a. Correction to "Robust optical features of fine mode size distributions: application to the Québec smoke event of 2002". *J. Geophys. Res.* 113, D24203.
- O'Neill, N.T., Pancrati, O., Baibakov, K., Eloranta, E., Batchelor, R.L., Freemantle, J., McArthur, L.J.B., Strong, K., Lindenmaier, R., 2008b. Occurrence of weak, sub-micron, tropospheric aerosol events at high Arctic latitudes. *Geophys. Res. Lett.* 35.
- Pérez-Ramírez, D., Aceituno, J., Ruiz, B., Olmo, F., Alados-Arboledas, L., 2008. Development and calibration of a star photometer to measure the aerosol optical depth: smoke observations at a high mountain site. *Atmos. Environ.* 42, 2733–2738.
- Pérez-Ramírez, D., Lyamani, H., Olmo, F.J., Whiteman, D.N., Alados-Arboledas, L., 2012. Columnar aerosol properties from sun-and-star photometry: statistical comparisons and day-to-night dynamic. *Atmos. Chem. Phys.* 12, 9719–9738.
- Pérez-Ramírez, D., Veselovskii, I., Whiteman, D.N., Suvorina, A., Korenskiy, M., Kolgotin, A., Holben, B., Dubovik, O., Siniuk, A., Alados-Arboledas, L., 2015. High temporal resolution estimates of columnar aerosol microphysical parameters from spectrum of aerosol optical depth by linear estimation: application to long-term AERONET and star-photometry measurements. *Atmos. Meas. Tech.* 8, 3117–3133.
- Queface, A.J., Piketh, S.J., Eck, T.F., Tsay, S.-C., Mavume, A.F., 2011. Climatology of aerosol optical properties in Southern Africa. *Atmos. Environ.* 45, 2910–2921.
- Reid, J.S., Hobbs, P.V., Ferek, R.J., Blake, D.R., Martins, J.V., Dunlap, M.R., Liousse, C., 1998. Physical, chemical, and optical properties of regional hazes dominated by smoke in Brazil. *J. Geophys. Res.* 103.
- Reid, J.S., Eck, T.F., Christopher, S.A., Hobbs, P.V., Holben, B.N., 1999. Use of the Angstrom exponent to estimate the variability of optical and physical properties of aging smoke particles in Brazil. *J. Geophys. Res.* 104.
- Reid, J.S., Eck, T.F., Christopher, S.A., Koppmann, R., Dubovik, O., Eleuterio, D.P., Holben, B.N., Reid, E.A., Zhang, J., 2005a. A review of biomass burning emissions part III: intensive optical properties of biomass burning particles. *Atmos. Chem. Phys.* 5, 827–849.
- Reid, J.S., Koppmann, R., Eck, T.F., Eleuterio, D.P., 2005b. A review of biomass burning emissions part II: intensive physical properties of biomass burning particles. *Atmos. Chem. Phys.* 5, 799–825.
- Remy, S., Kaiser, J.W., 2014. Daily global fire radiative power fields estimation from one or two MODIS instruments. *Atmos. Chem. Phys.* 14, 13377–13390.
- Sayer, A.M., Hsu, N.C., Eck, T.F., Smirnov, A., Holben, B.N., 2014. AERONET-based models of smoke-dominated aerosol near source regions and transported over oceans, and implications for satellite retrievals of aerosol optical depth. *Atmos. Chem. Phys.* 14, 11493–11523.
- Schafer, J.S., Eck, T.F., Holben, B.N., Artaxo, P., Duarte, A.F., 2008. Characterization of the optical properties of atmospheric aerosols in Amazonia from long-term AERONET monitoring (1993–1995 and 1999–2006). *J. Geophys. Res.* 113.
- Schwikowski, M., Brüttsch, S., Gäggeler, H.W., Schotterer, U., 1999. A high-resolution air chemistry record from an alpine ice core: fiescherhorn glacier, Swiss Alps. *J. Geophys. Res. Atmos.* 104, 13709–13719.
- Smirnov, A., Holben, B.N., Eck, T.F., Dubovik, O., Slutsker, I., 2000. Cloud-screening and quality control algorithms for the AERONET database. *Remote Sens. Environ.* 73, 337–349.
- Sinyuk, A., Holben, B.N., Smirnov, A., Eck, T.F., Slutsker, I., Schafer, J.S., Giles, D.M., Sorokin, M., 2012. Assessment of error in aerosol optical depth measured by AERONET due to aerosol forward scattering. *Geophys. Res. Lett.* 39, L23806.
- Stein, A.F., Draxler, R.R., Rolph, G.D., Stunder, B.J.B., Cohen, M.D., Ngan, F., 2015.

- NOAA's HYSPLIT atmospheric transport and dispersion modeling system. *Bull. Am. Meteorological Soc.* 96, 2059–2077.
- Swap, R.J., Annegarn, H.J., Suttles, J.T., King, M.D., Platnick, S., Privette, J.L., Scholes, R.J., 2003. Africa burning: a thematic analysis of the southern African regional science initiative (SAFARI 2000). *J. Geophys. Res. Atmos.* 108 n/a–n/a.
- Torres, O., Chen, Z., Jethva, H., Ahn, C., Freitas, S.R., Barthia, P.K., 2010. OMI and MODIS observations of the anomalous 2008–2009 Southern Hemisphere biomass burning seasons. *Atmos. Chem. Phys.* 10, 3505–3513.
- Uhl, C., Kauffman, J.B., Cummings, D.L., 1998. Fire in Venezuelan Amazon 2: environmental conditions necessary for forest fires in the evergreen rainforest of Venezuela. *Oikos* 53, 176–184.
- Ulke, A.G., Longo, K.M., Freitas, S.R., 2011. Biomass burning in south America: transport patterns and impacts. In: Matovic, D. (Ed.), *Biomass - Detection, Production and Usage*.
- Uriarte, M., Yackulic, C.B., Cooper, T., Flynn, D., Cortes, M., Crk, T., Cullman, G., McGinty, M., Sircely, J., 2009. Expansion of sugarcane production in São Paulo, Brazil: implications for fire occurrence and respiratory health. *Agric. Ecosyst. Environ.* 132, 48–56.
- van der Werf, G.R., Randerson, J.T., Giglio, L., Collatz, G.J., Mu, M., Kasibhatla, P.S., Morton, D.C., DeFries, R.S., Jin, Y., van Leeuwen, T.T., 2010. Global fire emissions and the contribution of deforestation, savanna, forest, agricultural, and peat fires (1997–2009). *Atmos. Chem. Phys.* 10, 11707–11735.
- Van Marle, M.J.E., Field, R., van der Werf, G.R., Estrada de Wagt, I.A., Houghton, R.A., Rizzo, L.V., Artaxo, P., Tsigaridis, K., 2016. Fire and deforestation dynamics in Amazonia (1973–2014). *Glob. Biogeochem. Cycles* 31. <http://dx.doi.org/10.1002/2016GB005445>.
- Vedal, S., Dutton, S.J., 2006. Wildfire air pollution and daily mortality in a large urban area. *Environ. Res.* 102, 29–35.
- Veselovskii, I., Whiteman, D.N., Kolgotin, A., Andrews, E., Korenskii, M., 2009. Demonstration of aerosol property profiling by multiwavelength lidar under varying relative humidity conditions. *J. Atmos. Ocean. Technol.* 26, 1543–1557.
- Veselovskii, I., Dubovik, O., Kolgotin, A., Korenskiy, M., Whiteman, D.N., Allakhverdiev, K., Huseyinoglu, F., 2012. Linear estimation of particle bulk parameters from multi-wavelength lidar measurements. *Atmos. Meas. Tech.* 5, 1135–1145.
- Veselovskii, I., Whiteman, D.N., Korenskiy, M., Kolgotin, A., Dubovik, O., Perez-Ramirez, D., Suvorina, A., 2013. Retrieval of spatio-temporal distributions of particle parameters from multiwavelength lidar measurements using the linear estimation technique and comparison with AERONET. *Atmos. Meas. Tech.* 6, 2671–2682.
- Veselovskii, I., Whiteman, D.N., Korenskiy, M., Suvorina, A., Kolgotin, A., Lyapustin, A., Wang, Y., Chin, M., Bian, H., Kucsera, T.L., Pérez-Ramírez, D., Holben, B., 2015. Characterization of forest fire smoke event near Washington, DC in summer 2013 with multi-wavelength lidar. *Atmos. Chem. Phys.* 15, 1647–1660.
- Vuille, M., 1999. Atmospheric circulation over the Bolivian Altiplano during dry and wet periods and extreme phases of the southern oscillation. *Int. J. Climatol.* 19, 1579–1600.
- Ward, D.E., Susott, R.A., Kauffman, J.B., Babbitt, R.E., Cummings, D.L., Dias, B., Holben, B.N., Kaufman, Y.J., Rasmussen, R.A., Setzer, W., 1992. Smoke and fire characteristics for cerrado and deforestation burns in Brazil: BASE-B experiment. *J. Geophys. Res.* 97, 14601–14619.
- Wonsick, M.M., Pinker, R.T., Ma, Y., 2014. Investigation of the “elevated heat pump” hypothesis of the Asian monsoon using satellite observations. *Atmos. Chem. Phys.* 14, 8749–8761.
- Xu, Y., Ramanathan, V., Washington, W.M., 2016. Observed high-altitude warming and snow cover retreat over Tibet and the Himalayas enhanced by black carbon aerosols. *Atmos. Chem. Phys.* 16, 1303–1315.
- Zieger, P., Kienast-Sjögren, E., Starace, M., von Bismarck, J., Bukowiecki, N., Baltensperger, U., Wienhold, F.G., Peter, T., Ruhtz, T., Collaud Coen, M., Vuilleumier, L., Maier, O., Emili, E., Popp, C., Weingartner, E., 2012. Spatial variation of aerosol optical properties around the high-alpine site Jungfraujoch (3580 m a.s.l.). *Atmos. Chem. Phys.* 12, 7231–7249.